

## ARTICLE OPEN



# Fatty acid desaturation by stearoyl-CoA desaturase-1 controls regulatory T cell differentiation and autoimmunity

Elien Grajchen<sup>1,2,13</sup>, Melanie Loix<sup>1,2,13</sup>, Paulien Baeten<sup>2,3</sup>, Beatriz F. Côte-Real<sup>1,2,4</sup>, Ibrahim Hamad<sup>1,2,4</sup>, Sam Vanherle<sup>1,2</sup>, Mansour Haidar<sup>1,2</sup>, Jonas Dehairs<sup>5</sup>, Jelle Y. Broos<sup>6,7</sup>, James M. Ntambi<sup>8</sup>, Robert Zimmermann<sup>9,10</sup>, Rolf Breinbauer<sup>10,11</sup>, Piet Stinissen<sup>1,2</sup>, Niels Hellings<sup>2,3</sup>, Sanne G. S. Verberk<sup>1,2</sup>, Gijs Kooij<sup>6</sup>, Martin Giera<sup>12</sup>, Johannes V. Swinnen<sup>5</sup>, Bieke Broux<sup>12,3,12</sup>, Markus Kleinewietfeld<sup>12,4</sup>, Jerome J. A. Hendriks<sup>1,2,14</sup> and Jeroen F. J. Bogie<sup>1,2,14</sup>✉

© The Author(s) 2023

The imbalance between pathogenic and protective T cell subsets is a cardinal feature of autoimmune disorders such as multiple sclerosis (MS). Emerging evidence indicates that endogenous and dietary-induced changes in fatty acid metabolism have a major impact on both T cell fate and autoimmunity. To date, however, the molecular mechanisms that underlie the impact of fatty acid metabolism on T cell physiology and autoimmunity remain poorly understood. Here, we report that stearoyl-CoA desaturase-1 (SCD1), an enzyme essential for the desaturation of fatty acids and highly regulated by dietary factors, acts as an endogenous brake on regulatory T-cell (Treg) differentiation and augments autoimmunity in an animal model of MS in a T cell-dependent manner. Guided by RNA sequencing and lipidomics analysis, we found that the absence of *Scd1* in T cells promotes the hydrolysis of triglycerides and phosphatidylcholine through adipose triglyceride lipase (ATGL). ATGL-dependent release of docosahexaenoic acid enhanced Treg differentiation by activating the nuclear receptor peroxisome proliferator-activated receptor gamma. Our findings identify fatty acid desaturation by SCD1 as an essential determinant of Treg differentiation and autoimmunity, with potentially broad implications for the development of novel therapeutic strategies and dietary interventions for autoimmune disorders such as MS.

**Keywords:** Regulatory T cells; Autoimmunity; Fatty acid metabolism; Stearoyl-CoA desaturase-1; Multiple sclerosis

*Cellular & Molecular Immunology* (2023) 20:666–679; <https://doi.org/10.1038/s41423-023-01011-2>

## INTRODUCTION

Autoimmunity reflects an imbalance between effector and regulatory mechanisms, resulting in loss of immunological self-tolerance. Multiple sclerosis (MS) is a devastating neurological disease and one of the most prevalent autoimmune disorders in the Western world. The autoimmune response in MS is characterized by an increase in autoreactive pro-inflammatory immune cell subsets, e.g., T helper (Th) 17 and Th1 cells, and a decrease in the number and function of regulatory T cells (Tregs) [1–3]. This imbalance between pathogenic and protective T cell subsets is considered to drive demyelination and neurodegeneration in the central nervous system (CNS). Hence, restoring the immune balance in favor of protective T cell subsets represents a promising strategy to halt or limit MS disease progression.

Emerging evidence indicates that fatty acids control adaptive immunity and MS disease pathology [4]. Early epidemiological studies found a strong association between excessive fat intake,

obesity, and the etiology of MS [5, 6]. Notwithstanding, the direct effects of dietary fatty acids on immune cell function and CNS pathology have only recently been uncovered. Carbon chain length and degree of desaturation appear to be key determinants that dictate the immunopathological outcome of dietary fatty acids in MS, with saturated short-chain, monounsaturated long-chain, and polyunsaturated very long-chain fatty acids inducing protective immunity and reducing CNS pathology [7–10]. Several recent studies have also defined the importance of endogenous fatty acid metabolic pathways in immune cell physiology. For example, the formation of specialized proresolving lipid mediators was found to be essential for inducing a protective adaptive immune response [11, 12]. Furthermore, inhibition of de novo fatty acid synthesis and stimulation of beta-oxidation attenuate neuroinflammation and favor the differentiation of Tregs at the expense of Th17 cells [13–18]. Here, changes in the metabolism and intracellular levels of oleic (C18:1)

<sup>1</sup>Department of Immunology and Infection, Biomedical Research Institute, Hasselt University, Diepenbeek, Belgium. <sup>2</sup>University MS Center Hasselt, Pelt, Belgium. <sup>3</sup>Neuro-Immune Connections and Repair Lab, Department of Immunology and Infection, Biomedical Research Institute, Hasselt University, Diepenbeek, Belgium. <sup>4</sup>VIB Laboratory of Translational Immunomodulation, VIB Center for Inflammation Research, Hasselt University, Diepenbeek, Belgium. <sup>5</sup>Department of Oncology, Laboratory of Lipid Metabolism and Cancer, LKI – Leuven Cancer Institute, KU Leuven - University of Leuven, Leuven, Belgium. <sup>6</sup>Department of Molecular Cell Biology and Immunology, Amsterdam University Medical Center, Vrije Universiteit Amsterdam, Amsterdam Neuroscience, MS Center Amsterdam, Amsterdam, The Netherlands. <sup>7</sup>Center for Proteomics and Metabolomics, Leiden University Medical Center, Leiden, The Netherlands. <sup>8</sup>Department of Biochemistry, Department of Nutritional Sciences, University of Wisconsin-Madison, Madison, USA. <sup>9</sup>Institute of Molecular Biosciences, University of Graz, Graz, Austria. <sup>10</sup>BioTechMed-Graz, Graz, Austria. <sup>11</sup>Institute of Organic Chemistry, Graz University of Technology, Graz, Austria. <sup>12</sup>Cardiovascular Research Institute Maastricht, Department of Internal Medicine, Maastricht University, Maastricht, The Netherlands. <sup>13</sup>These authors contributed equally: Elien Grajchen, Melanie Loix. <sup>14</sup>These authors contributed equally: Jerome J. A. Hendriks, Jeroen F. J. Bogie. ✉email: jeroen.bogie@uhasselt.be

Received: 9 September 2022 Accepted: 23 March 2023

Published online: 12 April 2023

and palmitic acid (C16:0) triggered a neuroprotective adaptive immune response [13, 18].

In this study, we defined the importance of stearoyl-CoA desaturase-1 (SCD1), an enzyme that catalyzes the rate-limiting step in the conversion of saturated fatty acids (SFAs, C16:0 and C18:0) into mono-unsaturated fatty acids (MUFAs, C16:1 and C18:1), in T-cell physiology and neuroinflammation. SCD1 belongs to the family of  $\Delta 9$  fatty acid desaturases whose expression and activity are highly responsive to dietary factors and are negatively and positively regulated by polyunsaturated fatty acids (PUFAs) and Western-type diets rich in SFAs, respectively [4, 19]. We show that pharmacological inhibition of SCD1 and *Scd1* deficiency doubles peripheral Treg numbers and attenuates disease severity in experimental autoimmune encephalomyelitis (EAE), the most commonly used animal model to study MS. Guided by RNA sequencing and lipidomics analyses, we reveal that *Scd1* deficiency promotes Treg differentiation through adipose triglyceride lipase (ATGL)-dependent hydrolysis of triglycerides and phosphatidylcholine, thereby releasing nonesterified bioactive docosahexaenoic acid (DHA, C22:6), a natural ligand of the nuclear receptor peroxisome proliferator-activated receptor gamma (PPAR $\gamma$ ). Our findings highlight the importance of SCD1 in controlling Treg differentiation and reveal its potential as a therapeutic target for MS and other autoimmune diseases.

## MATERIALS AND METHODS

### Mice

*Scd1*-deficient (*Scd1*<sup>-/-</sup>) mice and mice with the third exon of the *Scd1* gene flanked by loxP sites (*Scd1*<sup>fl+/+</sup>) have been described in previous studies [20, 21]. Both mouse strains were backcrossed at least 10 times with C57BL/6 J mice. For generation of phagocyte-specific *Scd1*<sup>-/-</sup> mice, *Scd1*<sup>fl+/+</sup> mice were crossbred with C57BL/6 J *LysM*<sup>cre</sup> mice, which were kindly provided by Prof. Dr. Geert van Loo (VIB-UGent Center for Inflammation Research, University of Ghent, Belgium) [22]. All mice were genotyped by PCR, as previously described [21], or according to protocols established by Jackson Laboratories (United States, Bar Harbor). In all experiments using knockout mice, wild-type (wt) littermates were used as controls. For the experiment using phagocyte-specific knockout mice, *LysM*<sup>cre+/-</sup> and *Scd1*<sup>fl+/+</sup> mice were used as controls. For the adoptive transfer experiments, wt C57BL/6 J animals were purchased from Envigo (United States, Indianapolis). Mice were maintained on a 12 h light/dark cycle with free access to water and a standard chow diet.

### Experimental autoimmune encephalomyelitis (EAE)

At the age of 9–12 weeks, female mice were immunized subcutaneously with myelin oligodendrocyte glycoprotein peptide 35–55 (MOG<sub>35–55</sub>) emulsified in complete Freund's adjuvant with *Mycobacterium tuberculosis* according to the manufacturer's guidelines (EK-2110 kit; Hooke Laboratories, United States, Lawrence). Directly after immunization and after 24 h, the mice were intraperitoneally (i.p.) injected with 100 ng or 50 ng pertussis toxin (depending on lot number). Starting 5 days post-immunization, the mice with EAE were treated daily with an SCD1 inhibitor (CAY10566, 2.5 mg/kg, every 12 h by oral gavage), PPAR $\gamma$  inhibitor (GW9662, 2 mg/kg, every 24 h by i.p. injection), or vehicle (PBS for i.p., methylcellulose for oral gavage). Mice were weighed daily and clinically evaluated for neurological signs of the disease in a blinded fashion following a five-point standardized rating of clinical symptoms (0: no clinical symptoms; 1: tail paralysis; 2: tail paralysis and partial hind limb paralysis; 3: complete hind limb paralysis; 4: paralysis to the diaphragm; 5: death by EAE). For the adoptive transfer experiments, inguinal lymph nodes were isolated from donor mice with EAE at day 10 post-immunization. Single-cell suspensions were obtained by pushing the tissue through a 70  $\mu$ m cell strainer and subsequently cultured at  $7 \times 10^6$  cells/ml in stimulation medium consisting of RPMI-1640 with 0.5% penicillin/streptomycin (Gibco, United States, Massachusetts), 10% FCS (Gibco), 1% nonessential amino acid (NEAA; Sigma-Aldrich, United States, Burlington), 1% sodium pyruvate (Sigma-Aldrich), 20 ng/ml IL23 (BioLegend; United States, San Diego), and 20  $\mu$ g/ml rMOG<sub>35–55</sub> (Hooke Laboratories). After three days,  $10 \times 10^6$  cells were intraperitoneally injected into wt or *Scd1*<sup>-/-</sup> recipient mice, which were weighed and clinically evaluated for neurological signs of the disease on a daily basis and in a blinded fashion.

### Mouse T-cell cultures

CD4<sup>+</sup> T-cells were isolated ex vivo from the spleens of 9- to 12-week-old wt and *Scd1*<sup>-/-</sup> mice using the CD4<sup>+</sup> T-Cell Isolation Kit (Miltenyi Biotec; Germany, Cologne) according to the manufacturer's instructions. Next, live naive (CD4<sup>+</sup>CD25<sup>-</sup>CD44<sup>med</sup>CD62L<sup>+</sup>) T cells were obtained using a FACSAria cell sorter (BD Biosciences; United States, Franklin Lakes). The purity of the isolated cells was >95%. For Treg induction,  $0.75 \times 10^5$  naive T cells were cultured for one or two days with plate-bound anti-CD3 $\epsilon$  (2  $\mu$ g/ml, clone 145-2C11; BD Biosciences) in differentiation medium consisting of RPMI1640 with 1% penicillin/streptomycin, 10% FCS, 1% NEAA, 1% L-glutamine (Sigma-Aldrich), 50  $\mu$ M 2-mercaptoethanol (Gibco), anti-CD28 (2  $\mu$ g/ml, clone 37.51; BD Biosciences), and rmTGF $\beta$  for Treg differentiation (10 ng/ml; R&D Systems), IL12p70 (0.02  $\mu$ g/ml; R&D Systems) and dIL4 (10  $\mu$ g/ml; R&D Systems) for Th1 differentiation, dIFN $\gamma$  (10  $\mu$ g/ml; R&D Systems) and IL4 (0.01  $\mu$ g/ml; Preprotech) for Th2 differentiation, and rmTGF $\beta$  (10 ng/ml; R&D Systems) and IL6 (0.04  $\mu$ g/ml; R&D Systems) for Th17 differentiation in a 96-well U-bottom plate. SCD1 inhibitor (CAY10566, 1  $\mu$ M; Cayman Chemicals, United States, Michigan), ATGL inhibitor (Atglistatin, 20  $\mu$ M, synthesized as described previously [23]), nonesterified DHA (C22:6, 1  $\mu$ M; Cayman Chemicals), PPAR $\alpha$  antagonist (GW6471, 25  $\mu$ M; Sigma-Aldrich), PPAR $\beta$  antagonist (PT-S58, 25  $\mu$ M; Sigma-Aldrich), PPAR $\gamma$  antagonist (GW9662, 25  $\mu$ M; Sigma-Aldrich) or vehicle were added daily starting from the onset of cultures. DHA was dissolved in ethanol and complexed to fatty acid-free BSA (Sigma-Aldrich) in a 4:1 molar ratio. For determination of the lipidome after ATGL inhibition,  $0.75 \times 10^5$  *Scd1*<sup>-/-</sup> naive T cells were cultured for two days in RPMI-1640 with 1% penicillin/streptomycin, 10% FCS, 1% NEAA, 1% L-glutamine (Sigma-Aldrich), 50  $\mu$ M 2-mercaptoethanol (Gibco), and rmlL7 (10 ng/ml; Peprotech, United Kingdom, London) in a 96-well U-bottom plate. ATGL inhibitor or vehicle was added daily starting from the onset of culture.

The suppressive capacity of wt and *Scd1*<sup>-/-</sup> Tregs was assessed as described previously [24]. In brief, antigen presenting cells (APCs, CD4<sup>+</sup> effector T cells (Teff, CD4<sup>+</sup>CD25<sup>-</sup>), and Tregs (CD4<sup>+</sup>CD25<sup>+</sup>) were isolated ex vivo from spleens of 11-week-old wt and *Scd1*<sup>-/-</sup> animals using the CD4<sup>+</sup>CD25<sup>+</sup> Regulatory T-Cell Isolation Kit (Miltenyi Biotec) according to the manufacturer's instructions. The purity of the isolated cells was >95%. Increasing amounts of Tregs were cocultured alongside  $0.5 \times 10^5$  wt CFSE-labeled Teffs and  $2 \times 10^5$  irradiated wt APCs (30 Gy) in a 96-well V-bottom plate for three days. RPMI-1640 with 1% penicillin/streptomycin, 10% FCS, 1% NEAA, 1% L-glutamine, and 50  $\mu$ M 2-mercaptoethanol was used as culture medium. For characterization of the T cell compartment of wt and *Scd1*<sup>-/-</sup> animals with EAE, spleen and inguinal lymph nodes were isolated from the mice with EAE at day 10 post-immunization. Single-cell suspensions were obtained by pushing the tissue through a 70  $\mu$ m cell strainer and cultured overnight at  $5 \times 10^6$  cells/ml in culture medium (RPMI-1640 with 0.5% penicillin/streptomycin, 10% FCS, 1% NEAA, and 1% sodium pyruvate).

### Human T-cell cultures

Using density gradient centrifugation, peripheral blood mononuclear cells (PBMCs) were obtained from healthy donors and age- and gender-matched relapse-remitting MS patients (untreated). CD4<sup>+</sup>CD25<sup>-</sup> T cells were isolated using the CD4<sup>+</sup> T-Cell Isolation Kit (Miltenyi Biotec) and CD25 Microbeads (Miltenyi Biotec) according to the manufacturer's instructions. Next, recent thymic emigrated (CD4<sup>+</sup>CD127<sup>+</sup>CD31<sup>+</sup>, designated hereafter as naive) T cells were obtained using a FACSAria cell sorter (BD Biosciences). The purity of the isolated cells was >95%. For Treg induction,  $0.1 \times 10^6$  naive T cells were cultured for four days in differentiation medium consisting of RPMI-1640 with 0.5% penicillin/streptomycin, 10% FCS, 1% NEAA, 1% sodium pyruvate, IL2 (50 U/ml; Roche, Belgium, Brussels), rhTGF $\beta$  (5 ng/ml, Peprotech), soluble anti-CD3 $\epsilon$  (1.25  $\mu$ g/ml, clone OKT3; eBioscience, United States, San Diego), and Treg Suppression Inspector beads (Miltenyi Biotec) in a 96-well U-bottom plate. SCD1 inhibitor (CAY10566, 1  $\mu$ M), ATGL inhibitor (Atglistatin, 20  $\mu$ M, synthesized as described previously [23]), PPAR $\alpha$  antagonist (GW6471, 25  $\mu$ M; Sigma-Aldrich), PPAR $\beta$  antagonist (PT-S58, 25  $\mu$ M; Sigma-Aldrich), PPAR $\gamma$  antagonist (GW9662, 10  $\mu$ M), or vehicle was added daily starting from the onset of cultures.

The suppressive capacity of Tregs was assessed as described previously [25]. In brief, effector T cells (Teff, CD4<sup>+</sup>CD25<sup>-</sup>) were stained with CellTrace Violet (CTV, Thermo Fisher Scientific, 2.5  $\mu$ M) and cultured with Tregs (CD4<sup>+</sup>CD25<sup>+</sup>), which were differentiated in the presence of SCD1 inhibitor or vehicle. T cells were isolated using the CD4<sup>+</sup> T-Cell Isolation Kit (Miltenyi Biotec) and CD25 Microbeads (Miltenyi Biotec) according to the manufacturer's instructions. The purity of the isolated cells was >95%. Increasing amounts of Tregs were cocultured alongside  $0.5 \times 10^5$  Teff in a

96-well U-bottom plate for 5 days before being analyzed by FACS. RPMI-1640 with 0.5% penicillin/streptomycin, 10% FCS, 1% NEAA, 1% sodium pyruvate, IL2, rhTGF $\beta$ , and Treg Suppression Inspector beads was used as culture medium.

### shRNA-mediated gene silencing

Lentiviral particles were produced in HEK293T cells by cotransfecting with the packaging vector psPAX2 (8  $\mu$ g, Addgene, #12260), envelope vector pMD2.G (4  $\mu$ g, Addgene, #12259), and lentiviral vector (12  $\mu$ g, Mission Sigma) expressing the indicated specific shRNA or a control vector expressing an unspecific shRNA using 125 mM CaCl<sub>2</sub>. The specific shRNA clone for ATGL was TRCN0000249774. Supernatants were collected over the course of three days and filtered through a 0.45  $\mu$ m filter. Lentiviral particles were concentrated by ultracentrifugation for 2 h at 70,000  $\times$ g. Wt and *Scd1*<sup>-/-</sup> naïve T cells (0.75  $\times$  10<sup>5</sup> cells/well) were stimulated for one day prior to infection. Next, T cells were transduced with lentiviral particles at a lentiviral particle medium:culture medium ratio of 1:6. One day post-infection, naïve T cells were stimulated with rmTGF $\beta$  for Treg induction. Knockdown of endogenous ATGL was confirmed using flow cytometry.

### Cell lines

Jurkat T cells were cultured in RPMI 1640 with 0.5% penicillin/streptomycin, 10% FCS, and 1% L-glutamine.

### Flow cytometry

For the staining of spleen- and lymph node-derived lymphocytes, the following antibodies were used (all purchased from BioLegend): CD45 Alexa Fluor 700 (clone 30-F11, 1:200), CD3 FITC (clone 17A2, 1:200), CD4 Pacific Blue (clone GK1.5, 1:200), CD8 BV510 (clone 53-6.7, 1:200), IFN $\gamma$  PE-Cy7 (clone XMGI.2, 1:200), IL17 PE-Dazzle 594 (clone TC1-18H10.1, 1:200), IL4 PE (clone 11B11, 1:50), and FOXP3 Alexa Fluor 647 (clone MF-14, 1:200). For the isolation of mouse naïve T cells and the subsequent staining of differentiated Tregs, the following antibodies were used: CD4 PerCP-Cy5.5 (clone RM4-5, 1:100; BioLegend), CD44 APC-Cy7 (clone IM7, 1:100; BioLegend), CD25 PE-Cy7 (clone PC61, 1:200; BD Biosciences), CD62L APC (clone MEL1, 1:100; BioLegend), and FOXP3 eFluor450 (clone FJK-16s, 1:30; Invitrogen). For analysis of murine Treg suppressive capacity, the following antibodies were used: CD4 Pacific Blue (clone GK1.5, 1:200; BioLegend), CD25 PE-Cy7 (clone PC61, 1:200; BD Biosciences), and FOXP3 Alexa Fluor 647 (clone MF-14, 1:200; BioLegend). For analysis of ATGL abundance, the following antibody was used: ATGL (NB110-41536, 1:100; Novus, Belgium, Brugge). For the isolation of human naïve T cells and the subsequent staining of differentiated Tregs, the following antibodies were used: CD4 APC-eFluor780 (clone OKT4, 1:20; eBioscience), CD31 Alexa Fluor 488 (clone WM59, 1:20; BioLegend), CD127 PE (eBioRDR5, 1:20; Invitrogen), CD25 PE-Cy7 (clone M-A251, 1:40; BioLegend), and FOXP3 BV421 (clone 206D, 1:40; BioLegend). Dead cells were excluded by incubation with propidium iodide (1:250, BD Biosciences), Fixable Viability Dye eFluor506 (1:1000, Thermo Fisher Scientific), or Fixable Viability Dye Zombie NIR (1:1000, BioLegend). For analysis of surface markers, cells were stained in 1 $\times$  PBS containing 2% FCS and 0.1% azide. For staining of intracellular cytokines, cells were stimulated with phorbol 12-myristate 13-acetate (20 ng/ml; Sigma-Aldrich), calcium ionomycin (1  $\mu$ g/ml; Sigma-Aldrich), and Golgiplug (2  $\mu$ g/ml; BD Biosciences) for 4 h, and the FOXP3/transcription factor staining buffer set (Invitrogen) was used according to the manufacturer's instructions. Cells were acquired on an LSRFortessa Flow Cytometer (BD Biosciences).

### Quantitative PCR (qPCR)

Tissue or cells were lysed using QIAzol (Qiagen; The Netherlands, Roermond). RNA extraction and synthesis of complementary DNA were performed as described previously [26]. qPCR was subsequently conducted on a StepOnePlus or QuantStudio 3 detection system (Applied Biosystems; United States, Waltham). Data were analyzed using the  $\Delta\Delta$ Ct method and normalized to the most stable reference genes, as described previously [27]. Primer sequences are available on request.

### Immunofluorescence microscopy and image analysis

Cryosections were fixed in acetone for 10 min. Immunostaining and analysis of cryosections were performed as described previously [28]. The following antibodies were used: anti-CD3 (1:150; Bio-Rad, United States, Hercules), anti-F4/80 (1:100; Bio-Rad), anti-MBP (1:250; Sigma-Aldrich), and anti-SMI312 (1:250; BioLegend) combined with Alexa Fluor 555-labeled

anti-rat IgG and Alexa Fluor 488-labeled anti-mouse IgG secondary antibodies (1:400; Invitrogen, United States, Waltham). Analysis was carried out using a Nikon Eclipse 80i microscope and ImageJ software.

### Bulk RNA sequencing

Tissue or cells were lysed using QIAzol. RNA was extracted using the RNeasy mini kit (Qiagen). RNA samples were processed by the Genomics Core Leuven (Belgium). Total RNA content was analyzed with a Nanodrop 1000 spectrophotometer (Thermo Fisher Scientific), and RNA integrity was evaluated using a Bioanalyzer (Agilent). Sequencing libraries were generated using Lexogen's QuantSeq kit and sequenced on the Illumina HiSeq4000 sequencing system, generating 50 bp single-end reads. Splice-aware alignment was performed with STAR (v2.6.1b) using the default parameters [29]. Reads mapping to multiple loci in the reference genome were discarded. Quantification of reads per gene was performed with HT-seq Count v2.7.14. For count-based differential expression analysis of a single gene, the R-based Bioconductor package DESeq2 (The R Foundation for Statistical Computing) was used. Data are available as a GEO dataset under accession numbers GSE160040 and GSE224839. Differentially expressed genes were identified based on a log<sub>2</sub>-fold change < -0.5 and > 0.5 and a *P*-value < 0.05. The list of differentially expressed genes was used as the input for the analysis with Qiagen's Ingenuity Pathway Analysis (IPA, Qiagen).

### Liquid chromatography–electrospray ionization tandem mass spectrometry (LC–ESI–MS/MS)

Human PBMCs and CD4<sup>+</sup> T cells, and mouse naïve T cell pellets were reconstituted in 700  $\mu$ l of 1 $\times$  PBS and mixed with 800  $\mu$ l of 1 N hydrochloric acid:methanol (MeOH) 1:8 (v/v), 900  $\mu$ l of chloroform, 200  $\mu$ g/ml of the antioxidant 2,6-di-tert-butyl-4-methylphenol (BHT; Sigma-Aldrich), and 3  $\mu$ l of SPLASH LIPIDOMIX Mass Spec Standard (#330707; Avanti Polar Lipids, United States, Alabaster). After vortexing and centrifugation, the lower organic fraction was collected and evaporated using a Savant Speedvac spd111v (Thermo Fisher Scientific) at room temperature, and the remaining lipid pellet was stored at -20°C under argon. The lipid pellet was reconstituted in 100% ethanol. Lipid species were analyzed by LC–ESI–MS/MS on a Nexera X2 UHPLC system (Shimadzu, Japan, Kyoto) coupled with a hybrid triple quadrupole/linear ion trap mass spectrometer (6500+QTRAP system; AB SCIEX, The Netherlands, Nieuwerkerk aan den IJssel). Chromatographic separation was performed on an XBridge amide column (150 mm  $\times$  4.6 mm, 3.5  $\mu$ m; Waters) maintained at 35°C using mobile phase A [1 mM ammonium acetate in H<sub>2</sub>O-acetonitrile 5:95 (v/v)] and mobile phase B [1 mM ammonium acetate in H<sub>2</sub>O-acetonitrile 50:50 (v/v)] in the following gradient: (0–6 min: 0% B  $\rightarrow$  6% B; 6–10 min: 6% B  $\rightarrow$  25% B; 10–11 min: 25% B  $\rightarrow$  98% B; 11–13 min: 98% B  $\rightarrow$  100% B; 13–19 min: 100% B; 19–24 min: 0% B) at a flow rate of 0.7 ml/min, which was increased to 1.5 ml/min from 13 min onward. Sphingomyelin (SM), cholesteryl esters (CE), ceramides (CER), dihydroceramides (DCER), hexosylceramides (HCER), and lactosylceramides (LCER) were measured in positive ion mode with precursor scans of 184.1, 369.4, 264.4, 266.4, 264.4, and 264.4, respectively. Tri-, di-, and monoacylglycerides (TGs, DGs, and MGs) were measured in positive ion mode with a neutral loss scan for one of the fatty acyl moieties. Phosphatidylcholine (PC), lysophosphatidylcholine (LPC), phosphatidylethanolamine (PE), lysophosphatidylethanolamine (LPE), phosphatidylglycerol (PG), phosphatidylinositol (PI), and phosphatidylserine (PS) were measured in negative ion mode by fatty acyl fragment ions. Lipid quantification was performed by scheduled multiple reaction monitoring (MRM), and the transitions were based on neutral losses or typical product ions as described above. The instrument parameters were as follows: curtain gas = 35 psi; collision gas = 8 a.u. (medium); IonSpray voltage = 5500 V and -4500 V; temperature = 550°C; ion source gas 1 = 50 psi; ion source gas 2 = 60 psi; declustering potential = 60 V and -80 V; entrance potential = 10 V and -10 V; collision cell exit potential = 15 V and -15 V. Peak integration was performed with MultiQuant<sup>TM</sup> software version 3.0.3. Lipid species signals were corrected for isotopic contributions (calculated with Python Molmass 2019.1.1) and were quantified based on internal standard signals and adhered to the guidelines of the Lipidomics Standards Initiative (LSI; level 2 type quantification as defined by the LSI). Only the detectable lipid classes and fatty acyl moieties are reported in this manuscript.

### Liquid chromatography tandem mass spectrometry (LC–MS/MS)

Protein precipitation was performed on naïve T cells by dissolving them in 500  $\mu$ l of MeOH, to which 4  $\mu$ l of internal standard solution consisting of [<sup>2</sup>H<sub>4</sub>]LTB<sub>4</sub>, [<sup>2</sup>H<sub>8</sub>]15-HETE, [<sup>2</sup>H<sub>4</sub>]PGE<sub>2</sub>, and [<sup>2</sup>H<sub>5</sub>]DHA (50 ng/ml) was added.



Samples were placed at  $-20^{\circ}\text{C}$  for 20 min to equilibrate, after which they were spun down for 10 min (16,200 g at  $4^{\circ}\text{C}$ ). The supernatant was diluted with 2.5 ml of  $\text{H}_2\text{O}$ , and the pH was adjusted to 3.5 using formic acid (99%). Lipids were extracted using solid-phase extraction (SPE). In short, C18 cartridges (Sep-Pak, Vac3 3 cc (200 mg)) were equilibrated with MeOH (LC-MS grade, Merck) and  $\text{H}_2\text{O}$  (LC-MS grade, VWR Chemicals), after which the samples were loaded. Subsequently, cartridges were washed with  $\text{H}_2\text{O}$  (LC-MS grade) and *n*-hexane (Sigma-Aldrich), followed by elution using methylformate (spectrophotometric grade, Sigma-Aldrich). The elutes were then dried at  $40^{\circ}\text{C}$  using a gentle stream of nitrogen and reconstituted in 100  $\mu\text{l}$  of MeOH: $\text{H}_2\text{O}$  (40%). Next, samples were analyzed using a targeted LC-MS/MS method as described previously [30]. Here, chromatographic separation was accomplished using a Shimadzu LC system consisting of two LC-30AD pumps, a SIL-30AC autosampler, and a CTO-20AC column oven (Shimadzu). Compounds were separated on a Kinetex C18 column (50 mm  $\times$  2.1 mm, 1.7  $\mu\text{m}$ ) protected with a C8 precolumn (Phenomenex, United States, Torrance). Samples were eluted at a constant flow rate of 400  $\mu\text{l}/\text{min}$  with a gradient of  $\text{H}_2\text{O}$  (eluent A) and MeOH (eluent B), both with 0.01% acetic acid [30]. Other instrument parameters were in line with the protocol of Jónasdóttir et al. [30] and scheduled MRM mode was used to detect compounds. Compounds were identified using their relative retention times together with characteristic mass transitions. These and other individually optimized parameters can be found in Supplementary Table 1. Only detectable nonesterified fatty acids and downstream metabolites are reported in this manuscript.

### Luciferase-based nuclear receptor reporter assay

For determination of the ligation of PPAR $\alpha$ , PPAR $\beta$ , and PPAR $\gamma$ , luciferase-based reporter assays were performed using the ONE-Glo™ Luciferase Assay System kit (Promega, United States, Madison). Jurkat T cells were transfected with bacterial plasmid constructs expressing luciferase under control of the promoter region of the ligand-binding domain for PPAR $\alpha$ , PPAR $\beta$ , or PPAR $\gamma$ , which were kindly provided by Prof. Dr. Bart Staels (University of Lille, Inserm, France) [31, 32]. Cells were grown to 50–60% confluency in 60 mm plates, transfected with 1.8  $\mu\text{g}$  of plasmid DNA including 0.2  $\mu\text{g}$  pGAL4hPPAR $\alpha$ , pGAL4hPPAR $\beta$ , or pGAL4hPPAR $\gamma$ , 1  $\mu\text{g}$  pG5-TK-GL3, and 0.6  $\mu\text{g}$  of pCMV- $\beta$ -galactosidase, using JetPEI (Polyplus-transfection SA, France, Illkirch-Graffenstaden) as transfection reagent. Transfected cells were treated with SCD1 inhibitor (CAY10566, 10  $\mu\text{M}$ ), ATGL inhibitor (Atglistatin, 20  $\mu\text{M}$ ), nonesterified DHA (1  $\mu\text{M}$ ), PPAR $\alpha$  agonist (WY-14643, 10  $\mu\text{M}$ ; Sigma-Aldrich), PPAR $\beta$  agonist (GW501516, 10  $\mu\text{M}$ ; Sigma-Aldrich), PPAR $\gamma$  agonist (Rosiglitazone, 10  $\mu\text{M}$ ; Millipore), or vehicle for 24 h. Following treatment, cells were lysed in lysis buffer (25 mM glycyl-glycine, 15 mM  $\text{MgSO}_4$ , 4 mM EGTA, and 1x Triton; all from Sigma-Aldrich). For correction for transfection efficacy,  $\beta$ -galactosidase activity was measured using lysate diluted 1:10 in B-gal buffer, consisting of 20% 2-nitrophenyl  $\beta$ -D-galactopyranoside (ONPG; Sigma-Aldrich) and 80% Buffer Z (0.1 M  $\text{Na}_2\text{HPO}_4$ , 10 mM KCl, 1 mM  $\text{MgSO}_4$ , and 3.4  $\mu\text{l}/\text{ml}$  2-mercaptoethanol; all from Sigma-Aldrich). Luminescence and absorbance (410 nm) were measured using a FLUOstar Optima (BMG Labtech, Germany, Ortenberg).

### Statistics

Data were analyzed for statistical significance using GraphPad Prism and are reported as the mean  $\pm$  SEM. Data were tested for normal distribution using the d'Agostino and Pearson omnibus normality test. When datasets were normally distributed, ANOVA (Tukey's post hoc analysis) or a two-tailed unpaired Student's t-test (with Welch's correction if necessary) was used to determine statistical significance between groups. If datasets were not normally distributed, the Kruskal–Wallis or Mann–Whitney analysis was used. Significant differences were identified by *P*-values  $< 0.05$  (\**P*  $< 0.05$ , \*\**P*  $< 0.01$ , and \*\*\**P*  $< 0.001$ ).

### Study approval

All animal procedures were conducted in accordance with institutional guidelines and approved by the Ethical Committee for Animal Experiments of Hasselt University (ID201521, ID201611, ID201822, ID201828, ID201912K, ID201914). All experimental protocols using PBMCs were conducted in accordance with institutional guidelines and approved by the Medical Ethical Committee of Hasselt University (UH-IMMVET-P1). Written informed consent was obtained from all participants included in this study.

## RESULTS

### SCD1 deficiency and pharmacological inhibition reduce the severity of EAE by promoting Treg differentiation

Endogenous and dietary-induced changes in fatty acid metabolism have a major impact on MS disease progression [5–7, 9]. Given its essential role in controlling the desaturation of fatty acids, we defined the activity of SCD1 in peripheral blood mononuclear cells (PBMCs) and  $\text{CD4}^+$  T cells of untreated RR-MS patients and healthy controls. LC-ESI-MS/MS demonstrated increased 16:1/16:0 and 18:1/18:0 desaturation indices, a proxy for SCD1 activity, within the total lipidome of  $\text{CD4}^+$  T cells but not PBMCs (Fig. 1A). In-depth analysis further showed that  $\text{CD4}^+$  T cells of MS patients displayed enhanced desaturation in diglycerides (DG), phosphatidylglycerol (PG), and phosphatidylethanolamine-O (PE-O) (Fig. 1A). Having identified enhanced SCD1 activity in  $\text{CD4}^+$  cells of MS patients, we next sought to define its impact on autoimmunity. To this end, the experimental autoimmune encephalomyelitis (EAE) model, an experimental MS model, was employed. By using a mouse strain deficient in *Scd1* (*Scd1*<sup>−/−</sup>), we found that the absence of *Scd1* attenuated EAE disease severity and incidence and significantly delayed disease onset (Fig. 1B; Supplementary Fig. 1C, D). Pathologically, *Scd1*<sup>−/−</sup> mice showed a decreased inflammatory expression profile in their spinal cord compared to wt littermates, both at 18 days post-immunization and at their disease peaks (Fig. 1C). Accordingly, markedly reduced infiltration of  $\text{CD3}^+$  T cells and F4/80<sup>+</sup> phagocytes was observed in the spinal cord of the *Scd1*<sup>−/−</sup> mice with EAE at 18 dpi (Fig. 1D; Supplementary Fig. 1A). Consistent with a reduced neuroinflammatory burden, *Scd1*<sup>−/−</sup> deficiency attenuated demyelination in the spinal cord at 23 days post-immunization (Supplementary Fig. 2A, B). EAE disease was not associated with alterations in axonal integrity, nor did *Scd1*<sup>−/−</sup> deficiency affect this axonal parameter (Supplementary Fig. 2A, C). Comparable to those with *Scd1* deficiency, the animals treated with a pharmacological inhibitor of SCD1 (CAY10566) showed reduced EAE disease severity and incidence, delayed disease onset, and pathological parameters largely matched to those observed in the *Scd1*<sup>−/−</sup> mice (Fig. 1E–G; Supplementary Fig. 1E, F).

Previously, we demonstrated that *Scd1* deficiency induces a less-inflammatory, repair-promoting phenotype in macrophages and microglia in the CNS [26]. To assess whether these cells are responsible for reduced EAE disease severity in *Scd1*<sup>−/−</sup> mice, we induced EAE in mice with macrophage/microglia-specific *Scd1* deficiency (*Scd1*<sup>Fl/+</sup> *LysM*<sup>Cre/+</sup>). Interestingly, we found no difference in EAE disease severity, incidence, and onset between the wt and *Scd1*<sup>Fl/+</sup> *LysM*<sup>Cre/+</sup> mice (Fig. 1H; Supplementary Fig. 1G, H). These findings indicate that the attenuation of EAE symptoms by *Scd1* deficiency is not mediated by macrophages and microglia. To assess whether T cells are responsible for reduced EAE severity in *Scd1*<sup>−/−</sup> mice, we applied an adoptive transfer EAE model. For this purpose, lymph node-derived T lymphocytes were transferred from immunized wt or *Scd1*<sup>−/−</sup> mice to wt recipient mice. Strikingly, the animals that received *Scd1*<sup>−/−</sup> T cells showed almost no EAE symptoms compared to those transplanted with wt T cells (Fig. 1I; Supplementary Fig. 1I, J), mirroring the reduced demyelination in these animals (Supplementary Fig. 2A, D). No changes were observed in axonal integrity (Supplementary Fig. 2A, E). Notably, we observed no difference in EAE disease severity, incidence, and onset after transfer of wt T cells from immunized mice to wt or *Scd1*<sup>−/−</sup> mice (Fig. 1J; Supplementary Fig. 1K, L). Altogether, these findings indicate that the absence of SCD1 ameliorates EAE disease severity in a T cell-dependent manner.

To define the culprit T cell subset, we characterized the peripheral T cell compartment of the wt and *Scd1*<sup>−/−</sup> animals with EAE prior to disease onset. No differences were detected in the absolute number of lymph node immune cells between the wt and *Scd1*<sup>−/−</sup> animals (data not shown) or in the relative

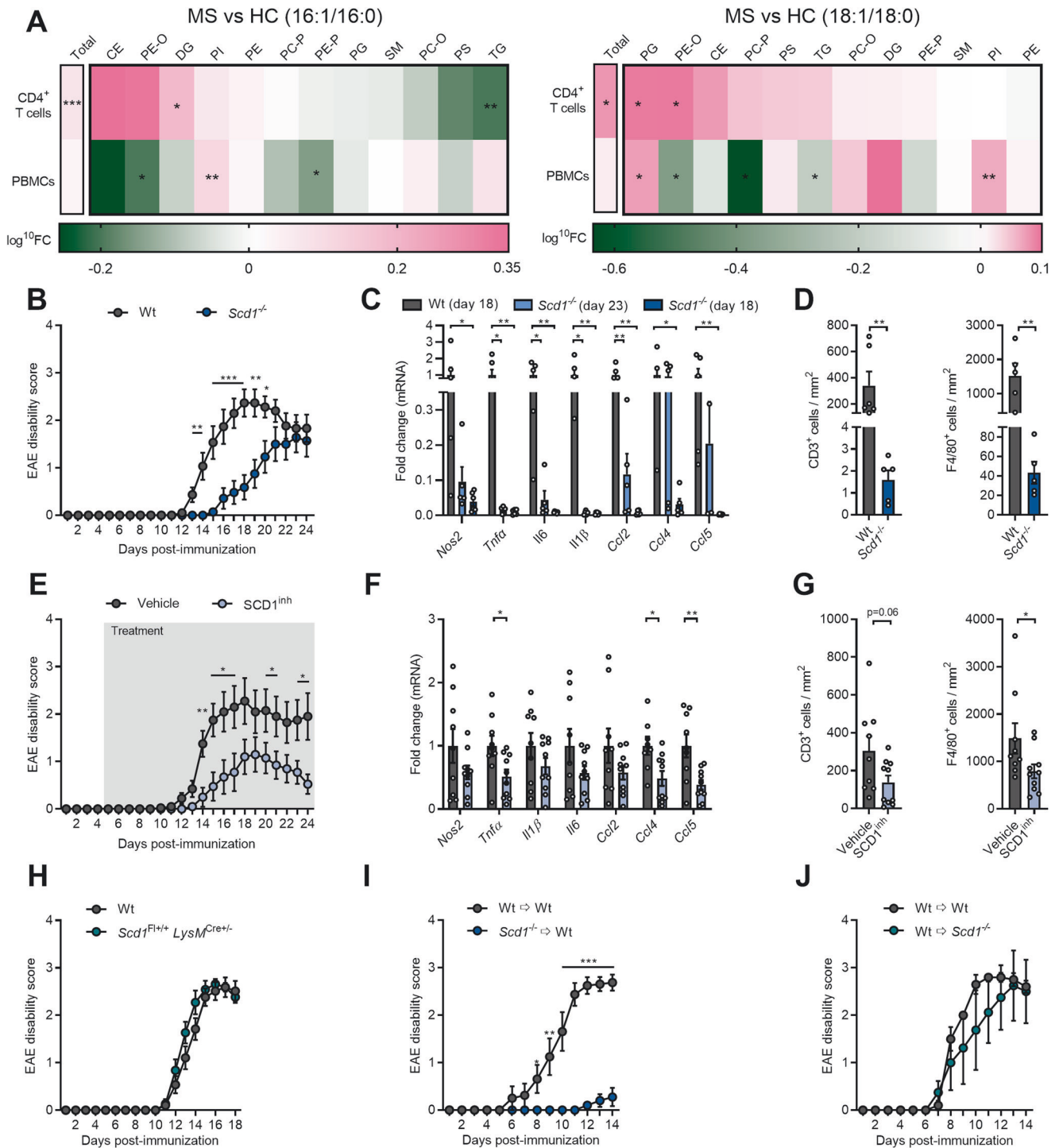


**Fig. 1** SCD1 inhibition and deficiency reduce EAE severity in a T cell-dependent manner. **A** Liquid chromatography–electrospray ionization tandem mass spectrometry (LC–ESI–MS/MS) analysis was performed to define the lipidome of peripheral blood mononuclear cells (PBMCs) and CD4<sup>+</sup> T cells from MS patients and age- and gender-matched healthy controls. Desaturation indices were determined by calculating the 16:1/16:0 and 18:1/18:0 ratios ( $n = 4$ ). **B** EAE disease score of *Scd1*<sup>-/-</sup> mice ( $n = 14$ ) and wild-type littermates (wt,  $n = 15$ ). **C** mRNA expression of *Nos2*, *Tnfa*, *Il1β*, *Il6*, *Ccl2*, *Ccl4*, and *Ccl5* in spinal cord tissue obtained from the wt ( $n = 6$ ) and *Scd1*<sup>-/-</sup> ( $n = 5$ ) animals with EAE (18 and 23 days post-immunization, dpi). **D** Quantification of CD3 and F4/80 staining of spinal cord tissue obtained from the wt ( $n = 6$ ) and *Scd1*<sup>-/-</sup> ( $n = 5$ ) animals with EAE at the peak of the disease (18 dpi). **E** EAE disease score of the wt mice treated with vehicle ( $n = 10$ ) or SCD1 inhibitor (SCD1<sup>inh</sup>, CAY10566, 2.5 mg/kg,  $n = 10$ ) by oral gavage twice a day with a 12 h interval. **F** mRNA expression of *Nos2*, *Tnfa*, *Il1β*, *Il6*, *Ccl2*, *Ccl4*, and *Ccl5* in spinal cord tissue obtained from the vehicle- ( $n = 9$ ) and SCD1 inhibitor-treated ( $n = 10$ ) animals with EAE (24 dpi). **G** Quantification of CD3 and F4/80 staining of spinal cord tissue obtained from the vehicle- ( $n = 9$ ) and SCD1 inhibitor-treated ( $n = 10$ ) animals with EAE (24 dpi). **H** EAE disease score of the wt (*Scd1*<sup>Fl/+</sup> and *LysM*<sup>Cre/+</sup>,  $n = 19$ ) and *Scd1*<sup>Fl/+</sup> *LysM*<sup>Cre/+</sup> ( $n = 11$ ) mice. **I** EAE disease score of the wt recipient mice that received lymph node-derived T lymphocytes from immunized wt (Wt → Wt,  $n = 8$ ) or *Scd1*<sup>-/-</sup> mice (*Scd1*<sup>-/-</sup> → Wt,  $n = 10$ ). **J** EAE disease score of the wt ( $n = 5$ ) and *Scd1*<sup>-/-</sup> ( $n = 4$ ) recipient mice that received lymph node-derived T lymphocytes from immunized wt animals. All replicates were biologically independent. All data are represented as the mean ± SEM and are pooled from 3 (**B**) or 2 (**E**, **H**, **I**) independent immunizations. \* $P < 0.05$ ; \*\* $P < 0.01$ ; \*\*\* $P < 0.001$ ; calculated with Tukey's post hoc analysis (**B**) or a two-tailed unpaired Student's t-test (**A**, **C**, **E**–**K**)

abundance of CD8<sup>+</sup> and CD4<sup>+</sup> T cells (Fig. 2A, B). Similarly, the frequency of the T helper subsets, e.g., CD4<sup>+</sup>IFN $\gamma$ <sup>+</sup> Th1 cells, CD4<sup>+</sup>IL17<sup>+</sup> Th17 cells, and CD4<sup>+</sup>IL4<sup>+</sup> Th2 cells, remained unaffected in *Scd1*<sup>-/-</sup> mice (Fig. 2A, B). Interestingly, we detected an increased frequency of CD4<sup>+</sup>FOXP3<sup>+</sup> Tregs in the lymph nodes of *Scd1*<sup>-/-</sup> mice (Fig. 2A, B). Similar findings were observed in the spleen of the wt and *Scd1*<sup>-/-</sup> animals with EAE (Fig. 2C; Supplementary Fig. 3A). To confirm the essential role of SCD1 in T cell physiology, we next assessed the impact of SCD1 on CD4<sup>+</sup> T cell subset differentiation in vitro. We observed that both genetic deficiency and pharmacological inhibition of SCD1 promoted the differentiation of Tregs from murine naïve T cells without affecting Th1, Th2, and Th17 cell differentiation (Fig. 2D; Supplementary Fig. 3B, D). A similar increase in Treg differentiation was observed using human PBMC-derived naïve T cells after exposure to the SCD1 inhibitor (Fig. 2E; Supplementary Fig. 3C). Of note, the absence or inhibition of SCD1 did not impact the suppressive capacity of mouse and human Tregs (Fig. 2F, G; Supplementary Fig. 4A, B), nor did it increase Treg proliferation (Supplementary Fig. 4C). Collectively, these findings show that SCD1 acts as a brake on the differentiation of Tregs without affecting their expansion and functional properties.

### **Scd1-deficient naïve T cells display a transcriptional profile characteristic of Tregs**

To identify transcriptional alterations that underlie the impact of *Scd1* deficiency on T cell physiology, we performed bulk RNA sequencing. Differential gene expression analysis revealed that 235 genes distinguished wt and *Scd1*<sup>-/-</sup> naïve CD4<sup>+</sup> T cells, with 135 upregulated and 100 downregulated in *Scd1*<sup>-/-</sup> naïve T cells (Fig. 3A; Supplementary Table 2). By using Ingenuity Pathway Analysis (IPA), we found that differentially expressed genes were highly associated with cancer and tumorigenic processes (Supplementary Fig. 5A), corresponding to the key role of SCD1 in cancer cell migration, metastasis, and tumor growth [33]. Canonical pathway analysis identified 34 enriched biological pathways (Supplementary Fig. 5B), including 'DHA signaling', 'unfolded protein response', and 'amyotrophic lateral sclerosis signaling' (Fig. 3B, C). Molecular and cellular functions that matched the transcriptional profile of naïve *Scd1*<sup>-/-</sup> T cells were mapped to phospholipid, cholesterol, and acylglycerol metabolism (Fig. 3D, E). These findings confirm the essential role of SCD1 in controlling cellular lipid metabolism.

Interestingly, 'conversion of Treg cells' was recognized as a key cellular process in naïve *Scd1*<sup>-/-</sup> T cells (Fig. 3D, E). Accordingly, based on the increased expression of *Foxp3*, *Ikzf2*, and *Rgs1*, upstream analysis demonstrated that the Treg-associated transcription factors FOXO1, FOXP3, C/EBP $\beta$ , and STAT5 are important upstream regulators of the transcriptional signature of naïve *Scd1*<sup>-/-</sup> T cells [34–37] (Fig. 3E, F). Elevated expression of Treg-associated genes such as *Foxp3*, *Ikzf2*, and *Rgs1* in naïve T cell cultures, as well as changes in the expression of other genes identified in the RNA sequencing analysis, were validated using qPCR (Fig. 3G, and Supplementary Fig. 5C). In contrast to naïve T cells, *Scd1*<sup>-/-</sup> Tregs did not show altered expression of *Foxp3*, *Ikzf2*, and *Rgs1* (Supplementary Fig. 6A), mirroring their unaltered suppressive function (Fig. 2F), nor did they demonstrate changes in the expression of metabolic genes that were differentially regulated in naïve wt and *Scd1*<sup>-/-</sup> T cells (Supplementary Fig. 6B). Likewise, bulk RNA sequencing demonstrated that wt and *Scd1*<sup>-/-</sup> early Tregs, which were induced by exposing naïve wt and *Scd1*<sup>-/-</sup> T cells to a Treg differentiation cocktail for a brief period of time (1 d), also did not display altered expression of these Treg-associated and metabolic genes (Supplementary Fig. 6C–E). Consistent with the latter, differentially expressed genes in early *Scd1*<sup>-/-</sup> Tregs no longer showed an overrepresentation in those pathways that IPA identified in naïve *Scd1*<sup>-/-</sup> T cells, including 'conversion of Treg cells', 'DHA signaling', and molecular and cellular functions related to phospholipid, cholesterol, and acylglycerol metabolism

(Supplementary Fig. 6F, G). In aggregate, these findings, together with the number of FOXP3<sup>+</sup> cells and FOXP3 protein abundance not differing between wt and *Scd1*<sup>-/-</sup> naïve T cells (Fig. 3H, I), suggest that *Scd1* deficiency induces a transcriptional profile characteristic of Tregs in naïve T cells without affecting the transcriptome of early or committed Tregs.

Chemical drugs and other molecule types associated with the transcriptome of naïve *Scd1*<sup>-/-</sup> T cells included cholesterol-reducing agents (pravastatin and simvastatin) and activators of the nuclear receptor PPAR $\gamma$  (rosiglitazone, docosahexaenoic acid, 10E, 12Z-octadecadienoic acid, prostaglandin E2, and 4-phenylbutyric acid) (Fig. 3J). The positive association between these lipid-modifying chemical drugs and fatty acid-containing lipid species confirms the pathway and functional enrichment analysis and further underlines the role of SCD1 in cellular lipid metabolism. In conclusion, pathway and gene set enrichment analyses indicate that *Scd1* deficiency in naïve T cells affects DHA and PPAR $\gamma$  signaling, alters phospholipid and triglyceride metabolism, and induces a transcriptional profile characteristic of Tregs.

### **Scd1 deficiency results in PUFA-depleted lysolecithin and triglycerides**

Given the overrepresentation of differentially expressed genes in pathways related to lipid metabolism, liquid chromatography-electrospray ionization tandem mass spectrometry (LC–ESI–MS/MS) analysis was performed to define the fatty acid lipidome of wt and *Scd1*<sup>-/-</sup> naïve T cells. Consistent with reduced SCD1 activity, naïve *Scd1*<sup>-/-</sup> T cells demonstrated decreased 16:1/16:0 and C18:1/C18:0 desaturation indices, particularly within phospholipid classes (Supplementary Fig. 7A, B). Of interest, naïve *Scd1*<sup>-/-</sup> T cells showed decreased levels of all major lipid classes except for lysophosphatidylcholine (LPC), a hydrolyzed derivative of phosphatidylcholine (PC; Fig. 4A, B; detailed information in Supplementary Fig. 7C–R), which argues for elevated hydrolysis of PC in naïve *Scd1*<sup>-/-</sup> T cells. The overall decrease in cellular lipids in naïve *Scd1*<sup>-/-</sup> T cells did not depend on reduced cell size or granularity (Supplementary Fig. 7S).

In-depth analysis further demonstrated that LPC in naïve *Scd1*<sup>-/-</sup> T cells was mainly depleted of the  $\omega$ 3 PUFA DHA (C22:6), aside from the expected decrease in palmitoleic acid (C16:1) (Fig. 4C). This decrease in DHA in LPC was not apparent in PC (Fig. 4D). Interestingly, mono-, di-, and triacylglycerides (MGs, DGs, and TGs) also showed a marked decrease in DHA (Fig. 4E), mirroring the enrichment of genes involved in the catabolism of acylglycerols in *Scd1*<sup>-/-</sup> naïve T cells (Fig. 3D). These findings point toward enhanced activity of a lipase that promotes the hydrolysis of PC and acylglycerols and favors the release of DHA in *Scd1*<sup>-/-</sup> naïve T cells. In support of the latter, LC–MS/MS analysis revealed an increased abundance of nonesterified DHA, alongside other PUFAs, in spleen tissue and naïve T cells from *Scd1*<sup>-/-</sup> animals (Fig. 4F). To identify the lipase involved, we re-evaluated differentially expressed genes obtained from our transcriptomic analysis. We found that the gene expression of *Pnpla2*, which encodes the enzyme adipose triglyceride lipase (ATGL), was elevated in naïve *Scd1*<sup>-/-</sup> T cells (Fig. 3C, E). Enhanced expression of ATGL in *Scd1*<sup>-/-</sup> naïve T cells was validated at the gene and protein levels (Fig. 4G, H). ATGL is a calcium-independent cellular phospholipase that hydrolyses TGs and phospholipids rich in DHA and arachidonic acid (AA) [38]. With respect to the latter, *Scd1*<sup>-/-</sup> T cells also showed a reduced abundance of AA in LPC and elevated levels of nonesterified AA (Fig. 4C, F). Collectively, these data suggest that *Scd1* deficiency enhances ATGL-mediated hydrolysis of PC and TGs, thereby releasing DHA and AA. Given that the release of phospholipid- and acylglycerol-associated DHA is essential for many of its biological activities as well as its capacity to activate nuclear receptors [39], the lipidomic analyses further provide a molecular rationale for the enrichment of genes in the DHA and PPAR $\gamma$  signaling pathways in *Scd1*<sup>-/-</sup> naïve T cells (Fig. 3B–E, J).



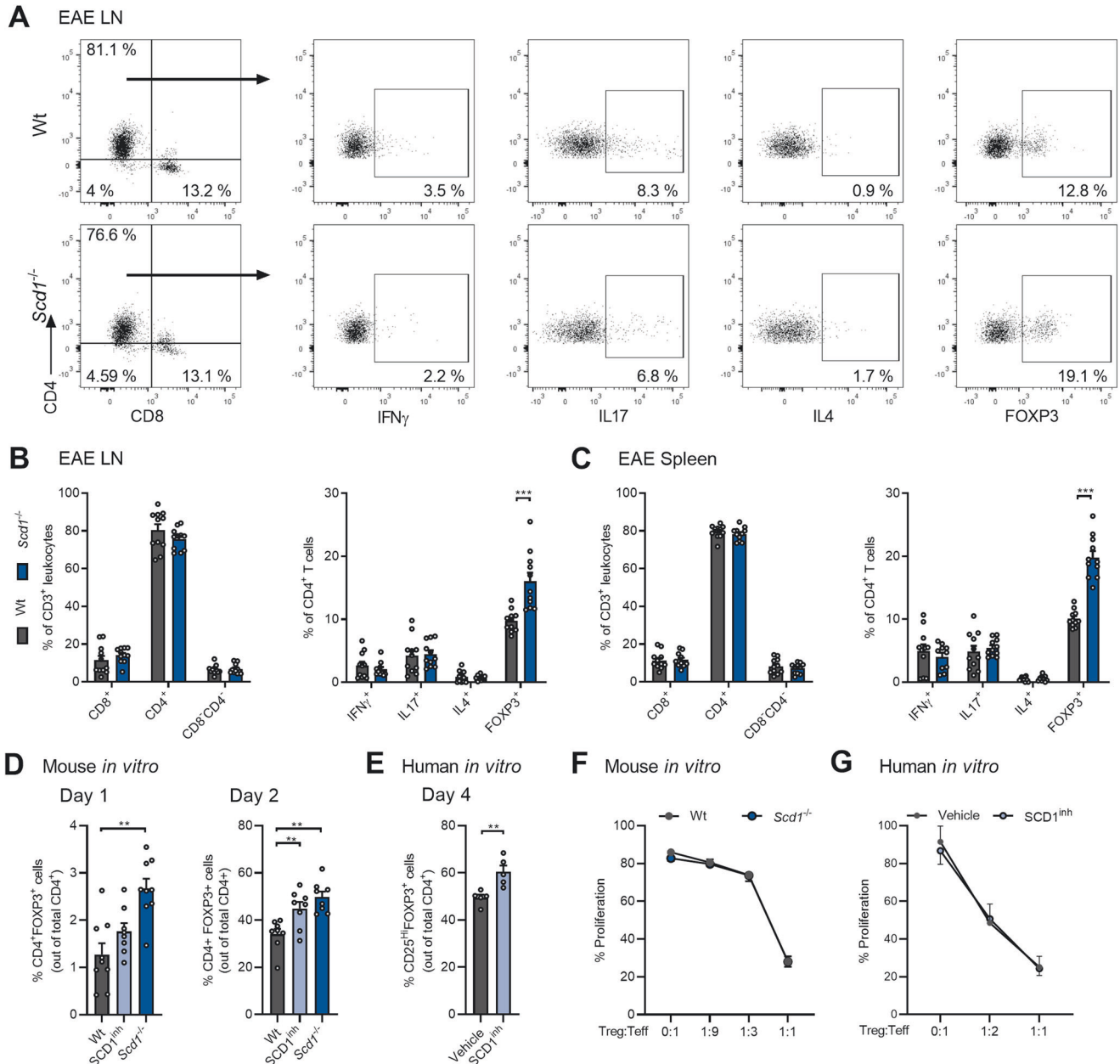


**Fig. 2** SCD1 deficiency and inhibition promote the differentiation of Tregs. **A–C** Frequency of CD4<sup>+</sup>, CD8<sup>+</sup>, CD4<sup>+</sup>CD8<sup>+</sup>, CD4<sup>+</sup>IFN $\gamma$ <sup>+</sup>, CD4<sup>+</sup>IL17<sup>+</sup>, CD4<sup>+</sup>IL4<sup>+</sup>, and CD4<sup>+</sup>FOXP3<sup>+</sup> cells in the lymph nodes (LN, **A**, **B**) and spleen (**C**) of wild-type (wt,  $n = 11$  animals) and *Scd1*<sup>-/-</sup> ( $n = 11$  animals) animals with EAE 10 days post-immunization (dpi). Representative flow cytometric plots (**A**) and flow cytometric analysis (**B**, **C**) are shown. **D**, **E** Wt and *Scd1*<sup>-/-</sup> mouse naïve T cells (**D**) and human naïve T cells (**E**) were differentiated under Treg polarizing conditions and treated with vehicle or SCD1 inhibitor (SCD1<sup>inh</sup>, CAY10566, 1  $\mu$ M). For mouse T-cell cultures, the frequency of CD4<sup>+</sup>FOXP3<sup>+</sup> cells was quantified one and two days after Treg induction ( $n = 8$  samples). For human T-cell cultures, the frequency of CD25<sup>hi</sup>FOXP3<sup>+</sup> cells was quantified four days after induction ( $n = 5$  healthy controls). The results from (**A–E**) are pooled from at least three independent experiments. **F**, **G** Suppressive capacity of wt and *Scd1*<sup>-/-</sup> mouse Tregs (**F**) or human Tregs differentiated in the presence of an SCD1 inhibitor (SCD1<sup>inh</sup>, CAY10566, 1  $\mu$ M) or vehicle (**G**). Increasing amounts of Tregs were cultured with CFSE- or CellTrace Violet (CTV)-labeled CD4<sup>+</sup>CD25<sup>-</sup> effector T cells (**F**,  $n = 3$  wt samples; **G**,  $n = 2$  healthy controls). Percentage proliferation was assessed after three (**F**) or five (**G**) days. All data are represented as the mean  $\pm$  SEM. \* $P < 0.05$ ; \*\* $P < 0.01$ ; \*\*\* $P < 0.001$ , calculated with two-tailed unpaired Student's t-test (**B**, **C**), Tukey's post hoc analysis (**D**), or Mann–Whitney analysis (**E–G**)

### ATGL-driven hydrolysis of PC and TGs stimulates Treg differentiation in *Scd1*<sup>-/-</sup> T cells by releasing DHA

Based on the RNA sequencing and lipidomic analysis, we next assessed the importance of ATGL and DHA in driving enhanced Treg differentiation of naïve *Scd1*<sup>-/-</sup> T cells. By using a pharmacological inhibitor of ATGL (Atglistatin), we found that ATGL inhibition partially counteracted the enhanced induction of Tregs from *Scd1*<sup>-/-</sup> naïve T cells in vitro (Fig. 5A, B) and, in parallel, markedly reduced the intracellular abundance of nonesterified

DHA (Supplementary Fig. 8A). ATGL inhibition did not decrease the capacity of wt naïve T cells to differentiate into Tregs (Fig. 5A, B). Similar findings were obtained following shRNA-mediated gene silencing of *Atgl* in mouse T cells and upon exposure of human PBMC-derived naïve T cells to the ATGL inhibitor (Fig. 5C–E; Supplementary Fig. 8B). In support of a key role of DHA in driving Treg differentiation, exposure to DHA significantly promoted Treg differentiation (Fig. 5F, G). Together, these data indicate that enhanced Treg differentiation upon SCD1 inhibition and in *Scd1*<sup>-/-</sup>

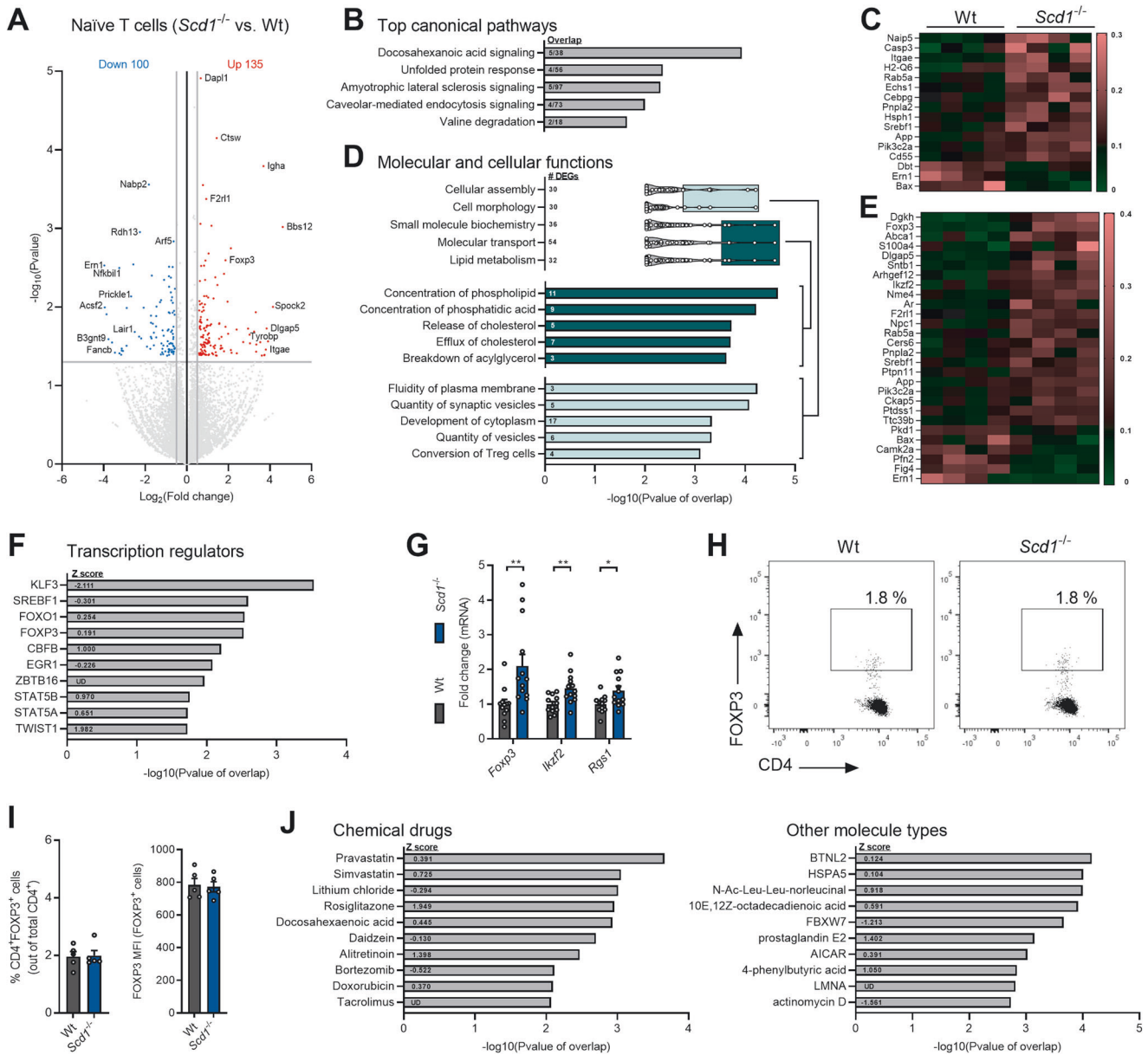


**Fig. 3 Naive *Scd1*<sup>-/-</sup> T cells display a transcriptional profile characteristic of Tregs.** **A–F, J** Bulk RNA sequencing was performed using wild-type (wt) and *Scd1*<sup>-/-</sup> naive CD4<sup>+</sup> T cells (CD4<sup>+</sup>CD25<sup>+</sup>CD44<sup>med</sup>CD62L<sup>+</sup>). **A** Differential gene expression analysis of the RNA sequencing data ( $\log_2$ -fold change < -0.5 and > 0.5; *P*-value < 0.05; complete list in Supplementary Table 2). **B** Top five most enriched canonical pathways in *Scd1*<sup>-/-</sup> naive T cells (complete list in Supplementary Fig. 3B). **C** Heatmap displaying the expression of genes present in the top five canonical pathways. The data were scaled by the sum of each row. **D** Molecular and cellular function categories associated with differentially expressed genes in *Scd1*<sup>-/-</sup> naive T cells. **E** Heatmap displaying the expression of genes involved in the molecular and cellular function categories. The data were scaled by the sum of each row. **F** Top 10 transcriptional regulators most associated with the transcriptome of *Scd1*<sup>-/-</sup> naive T cells. **G** mRNA expression of *Foxp3*, *Irf2*, and *Rgs1* in wt and *Scd1*<sup>-/-</sup> naive T cells (*n* = 11 samples). **H, I** The frequency of CD4<sup>+</sup>FOXP3<sup>+</sup> cells and the respective mean fluorescence intensity of FOXP3 in wt and *Scd1*<sup>-/-</sup> naive T-cell populations were quantified (*n* = 5 samples). Representative flow cytometric plots (**H**) and flow cytometric analysis (**I**) are shown. **J** Top 10 chemical drugs, transcriptional regulators, and other molecule types most associated with the transcriptome of *Scd1*<sup>-/-</sup> naive T cells. The results are pooled from four (**A–F, I, J**), seven (**G**), or five (**H**) independent experiments. Data from (**G, I**) are represented as the mean  $\pm$  SEM. \**P* < 0.05; \*\**P* < 0.01, calculated with two-tailed unpaired Student's *t*-test (**G, I**)

T cells partially relies on increased ATGL activity. They further suggest that nonesterified bioactive DHA, released through ATGL-mediated hydrolysis of PC and acylglycerols, acts as an important lipid metabolite in this pathway.

### Nonesterified DHA promotes Treg differentiation through PPAR $\gamma$

Upstream analysis revealed that differentially expressed genes in *Scd1*<sup>-/-</sup> naive T cells were associated with the activation of PPAR $\gamma$

(Fig. 3J). Consistent with these findings, naive *Scd1*<sup>-/-</sup> T cells demonstrated increased expression of PPAR $\gamma$ -responsive genes, including *Srebpc1*, *Abca1*, *Cd36*, *Cpt1a*, and *Lpl* (Supplementary Fig. 9A). Furthermore, by using ligand-binding luciferase reporter assays, we showed that SCD1 inhibition promoted the ligation of PPAR $\gamma$  but not PPAR $\alpha$  or PPAR $\beta$  (Fig. 6A). Interestingly, inhibition of ATGL countered the ligation of PPAR $\gamma$  induced by SCD1 inhibition (Fig. 6A). In line with a key role of nonesterified DHA in the activation of PPARs, exposure to DHA induced the activation



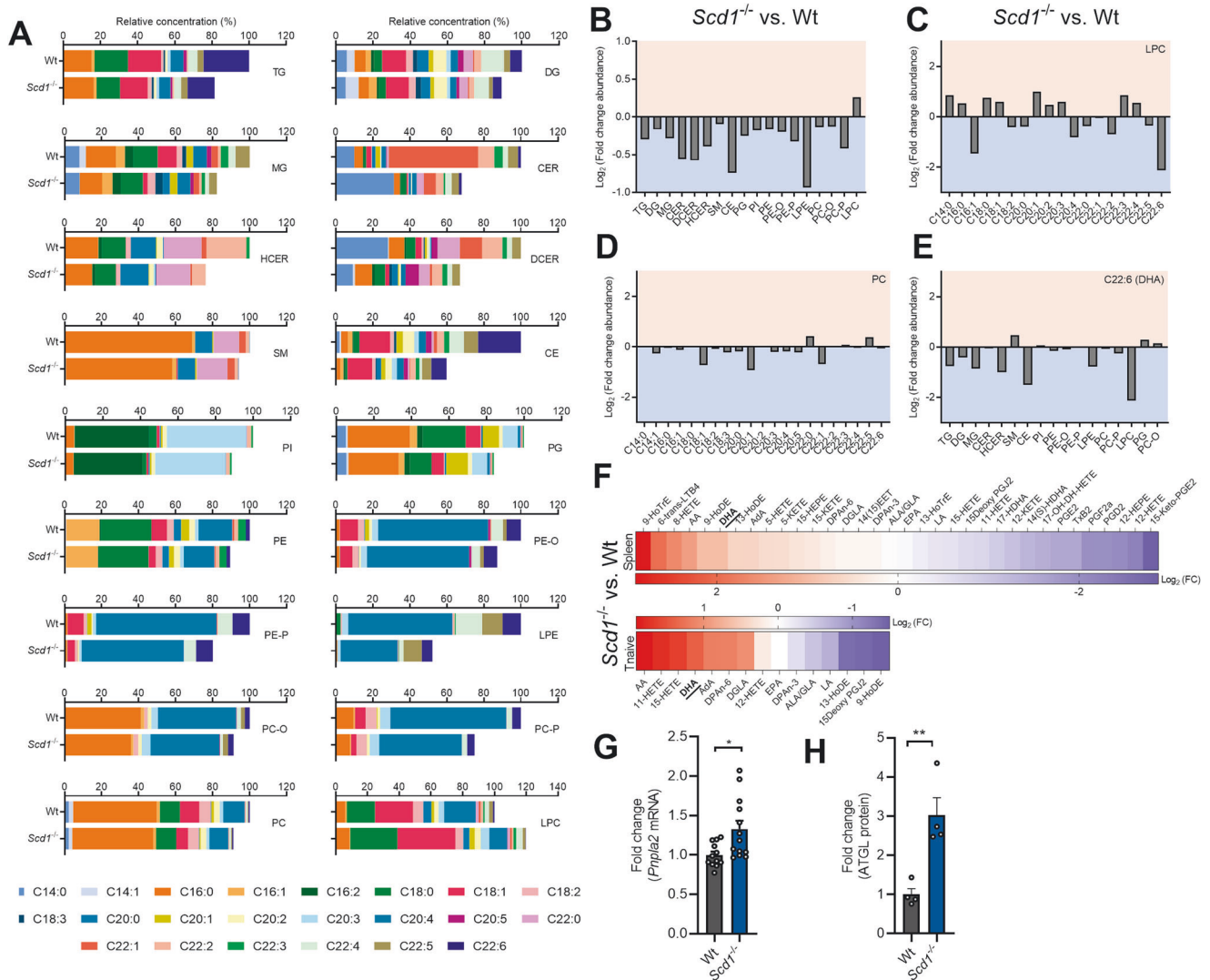


**Fig. 4** *Scd1* deficiency results in DHA-depleted lysolecithin and triglycerides. **A–E** Liquid chromatography–electrospray ionization tandem mass spectrometry (LC–ESI–MS/MS) analysis was performed to define the lipidome of wild-type (wt) and *Scd1*<sup>-/-</sup> naive T cells ( $n = 2$  samples). **A** Fatty acid composition of all lipid classes. **B–E** Log<sub>2</sub> fold change abundance of all lipid classes (**B**), fatty acyl moieties within lysophosphatidylcholine (LPC, **C**) and phosphatidylcholine (PC, **D**), and docosahexaenoic acid (DHA) within all lipid classes (**E**) is shown (*Scd1*<sup>-/-</sup> vs. wt). Only detectable fatty acyl moieties and nonesterified fatty acids and downstream metabolites are reported. **F** LC–MS/MS analysis was performed to determine the abundance of nonesterified fatty acids and downstream metabolites in wt and *Scd1*<sup>-/-</sup> naive T cells and spleen tissue ( $n = 3$  samples). Log<sub>2</sub> fold change abundance of all fatty acids and downstream metabolites is shown (*Scd1*<sup>-/-</sup> vs. wt). **G** mRNA expression of *Pnpla2* in wt and *Scd1*<sup>-/-</sup> naive T cells ( $n = 11$  samples). **H** ATGL protein levels in wt and *Scd1*<sup>-/-</sup> naive T cells ( $n = 4$  samples). The results are pooled from two (**A–E**, **H**), three (**F**), or seven (**G**) independent experiments. Data are represented as the mean (**A–F**) or as the mean  $\pm$  SEM (**G**). \* $P < 0.05$ ; \*\* $P < 0.01$ , calculated with two-tailed unpaired Student's t-test (**G**, **H**)

of PPAR $\gamma$  and PPAR $\beta$  but not PPAR $\alpha$  (Fig. 6B). Collectively, these findings strongly suggest that *Scd1* deficiency results in the ATGL-mediated release of DHA, which in turn activates PPAR $\gamma$ .

Given that PPAR $\gamma$  activation promotes Treg differentiation and that DHA is an endogenous PPAR $\gamma$  ligand [39–41], we next assessed the role of PPARs in driving enhanced Treg differentiation in *Scd1*<sup>-/-</sup> naive T cells. To this end, T cell cultures were exposed to well-described antagonists for the different PPAR isoforms (PPAR $\alpha$ <sup>anta</sup>: WY-14643; [42, 43] PPAR $\beta$ <sup>anta</sup>: PTS58; [44, 45] PPAR $\gamma$ <sup>anta</sup>: GW9662 [46]). Only PPAR $\gamma$  antagonism prevented enhanced mouse Treg differentiation induced by the absence of *Scd1* (Fig. 6C, D). Similar to murine T cells, treatment with the PPAR $\gamma$  antagonist reduced Treg differentiation independently of SCD1 and abolished enhanced Treg differentiation caused by SCD1 inhibition in human T cell cultures (Fig. 6E; Supplementary Fig. 9B).

Finally, to confirm the interplay between SCD1 and PPAR $\gamma$  in autoimmunity under physiological conditions, we exposed *Scd1*<sup>-/-</sup> animals with EAE to the PPAR $\gamma$  antagonist GW9662. Here, we observed that *Scd1* deficiency no longer reduced EAE disease severity in the presence of GW9662 compared to that of the control animals treated with GW9662 (Fig. 6F). Surprisingly, PPAR $\gamma$  antagonism reduced EAE disease severity compared to that of the control mice (Fig. 6F). The latter finding contradicts the protective impact of PPAR $\gamma$  agonists in the EAE model [47] but is consistent with GW9662 displaying anti-inflammatory properties in *in vitro* immune cell cultures and an LPS-triggered acute inflammation mouse model [48]. Consistent with changes in EAE disease severity, *Scd1*<sup>-/-</sup>-induced changes in CNS inflammation, accumulation of CD3<sup>+</sup> T cells, and demyelination were no longer apparent in the presence of GW9662 (Supplementary Fig. 9D–H). Furthermore, PPAR $\gamma$  antagonism reduced the observed increase in peripheral

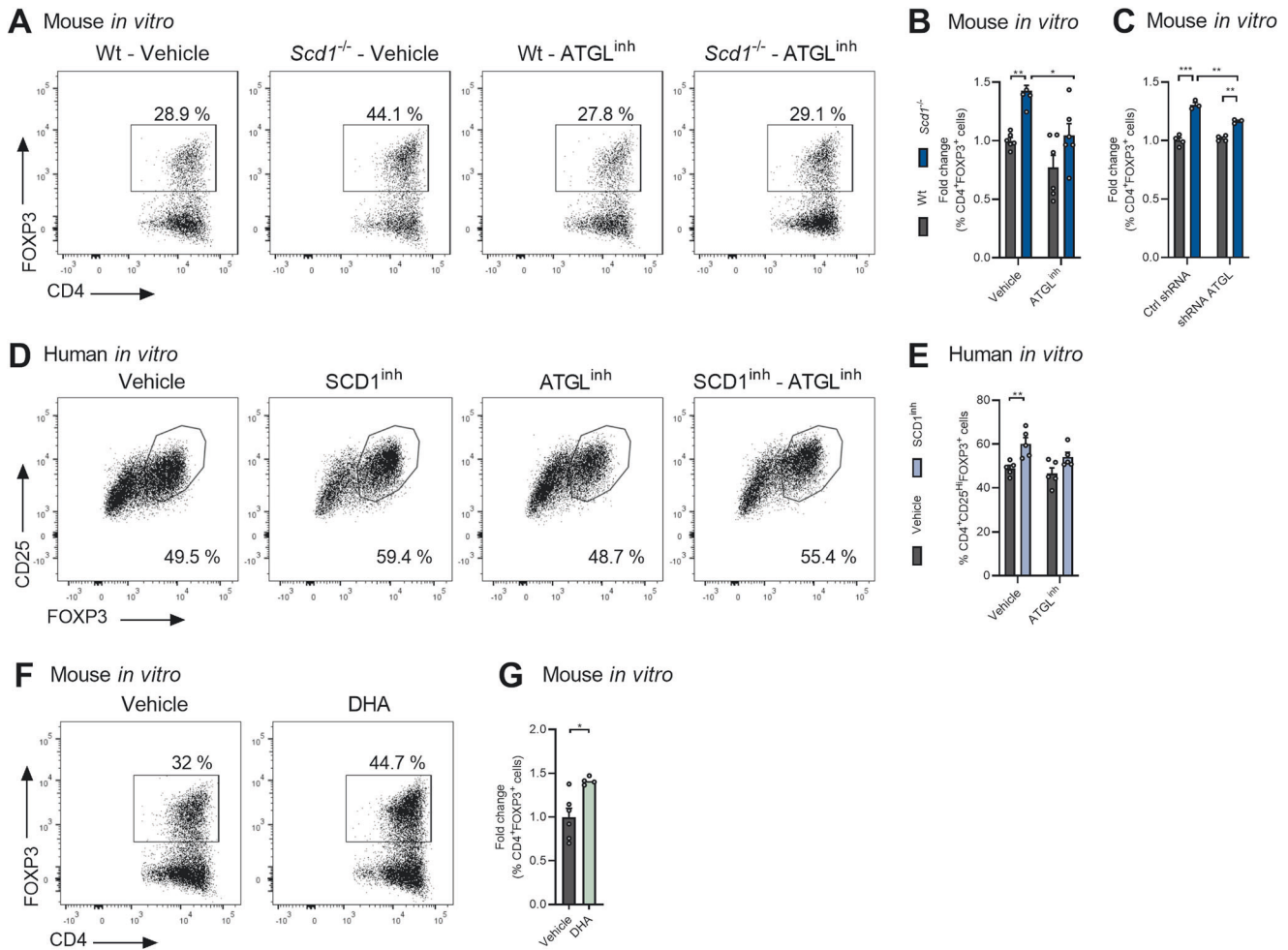


**Fig. 5** ATGL-driven release of nonesterified DHA enhances Treg differentiation in *Scd1*<sup>-/-</sup> T cells. **A–C** Wt and *Scd1*<sup>-/-</sup> mouse naïve T cells were differentiated under Treg polarizing conditions and treated with vehicle or ATGL inhibitor (ATGL<sup>inh</sup>, Atglistatin, 20  $\mu$ M;  $n = 9$  samples) or were transduced with ATGL-specific (shRNA ATGL) or control shRNA (Ctrl shRNA) ( $n = 4$  samples). The frequency of CD4<sup>+</sup>FOXP3<sup>+</sup> cells was quantified two days after Treg induction. **D, E** Human naïve T cells were treated with SCD1 inhibitor (SCD1<sup>inh</sup>, CAY10566, 1  $\mu$ M), ATGL<sup>inh</sup>, or vehicle ( $n = 5$  healthy controls). The frequency of CD25<sup>hi</sup>FOXP3<sup>+</sup> cells was quantified four days after Treg induction. Representative flow cytometric plots (**A, D**) and flow cytometric analyses (**B, C, E**) are shown. **F, G** Wt and *Scd1*<sup>-/-</sup> mouse naïve T cells were differentiated under Treg polarizing conditions and treated with vehicle or BSA-conjugated DHA (1  $\mu$ M;  $n = 4$  samples). The results are pooled from at least two independent experiments and presented as the mean  $\pm$  SEM. \* $P < 0.05$ ; \*\* $P < 0.01$ ; \*\*\* $P < 0.001$ , calculated with two-tailed unpaired Student's t-test (**B, C, E, G**)

Treg frequency in *Scd1*<sup>-/-</sup> animals with EAE (Fig. 6G; Supplementary Fig. 9C). These findings provide evidence that *Scd1* deficiency impacts EAE disease severity, neuroinflammation, and Treg differentiation through PPAR $\gamma$  under physiological conditions.

## DISCUSSION

An imbalance between pathogenic and protective T cell subsets is considered to propel autoimmunity. The findings from this study indicate that the FA desaturase SCD1 tightly controls T cell fate and autoimmunity and that its activity is increased in CD4<sup>+</sup> T cells of MS patients. We report that pharmacological inhibition and genetic deficiency of SCD1 stimulates Treg differentiation and, in parallel, attenuates neuroinflammation and disease severity in the EAE model in a T cell-dependent manner. We further provide evidence that *Scd1* deficiency promotes Treg differentiation through ATGL-dependent hydrolysis of TGs and PC, thereby releasing nonesterified bioactive DHA, a natural ligand of the nuclear receptor PPAR $\gamma$ . Thus, our findings identify an intricate relationship between FA desaturation, Treg differentiation, and autoimmunity.

FA metabolism is increasingly being acknowledged as a hub and driver of T cell physiology in health and disease [4, 11–18]. Our data indicate that the FA desaturase SCD1 acts as an endogenous brake on the differentiation of Tregs, thereby contributing to neuroinflammation in the EAE model. Consistent with our findings, previous studies showed that intracellular levels of substrates and products of SCD1, e.g., oleic acid (C18:1) and palmitic acid (C16:0), closely regulate T cell and Treg differentiation and maintenance [9, 13, 18]. Likewise, SCD1 inhibition was recently found to increase the frequency of follicular Tregs in the spleen following influenza immunization [49]. In contrast, *Scd1* deficiency accelerates and exacerbates the development of colitis by promoting the colitogenic potential of effector T cells [50]. Here, elevated levels of SFA increased cellular membrane fluidity and augmented the secretory profile of effector T cells. However, the authors did not assess the impact of *Scd1* deficiency on Treg physiology. Differences in the immunopathology and applied experimental animal models, e.g., adoptive transfer of naïve or antigen-sensitized T cells to *Rag1*<sup>-/-</sup> and wt mice, respectively, might well explain the opposing outcome of *Scd1* deficiency on disease initiation and severity in the colitis and EAE model.

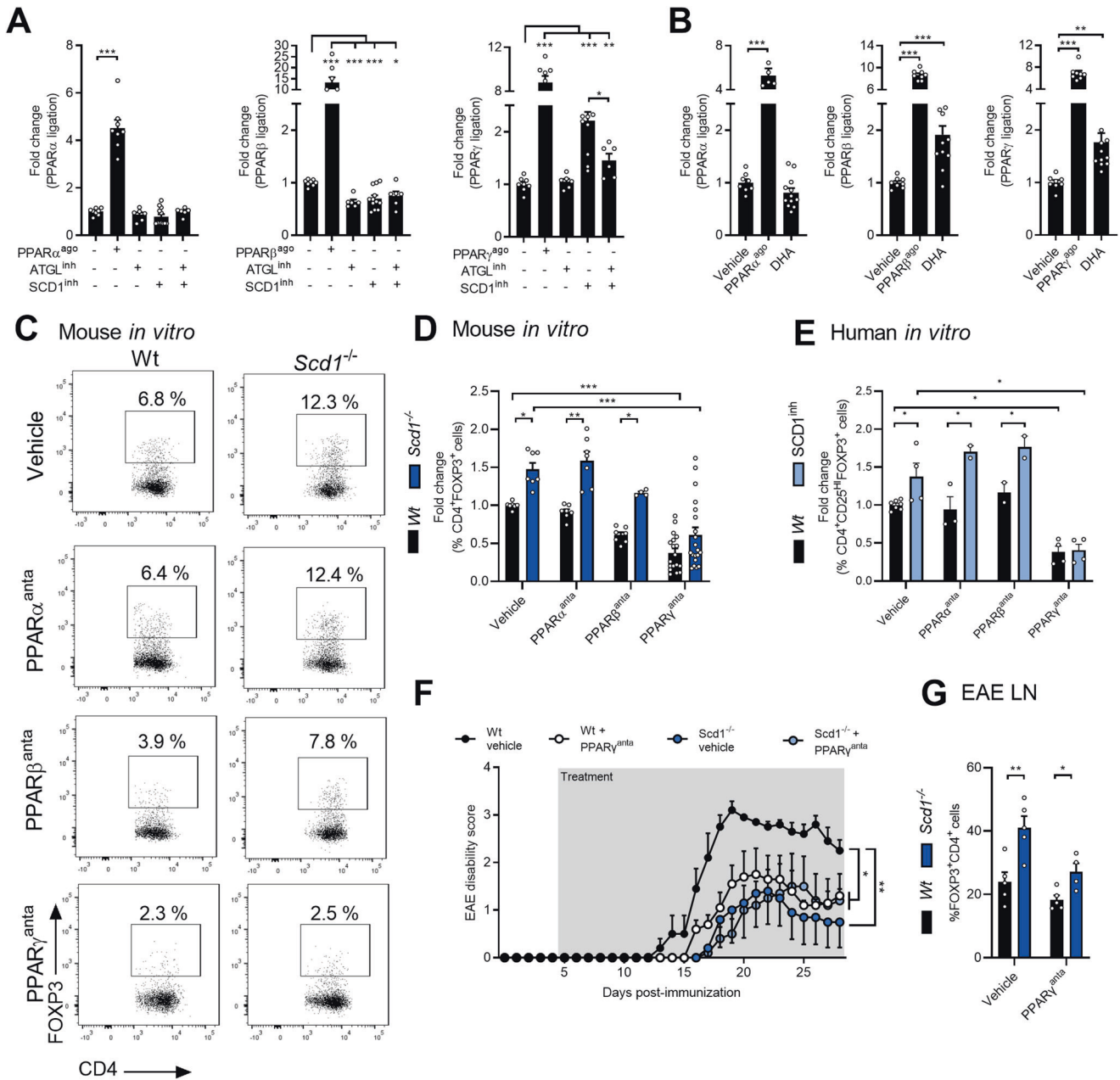


**Fig. 6** DHA-PPAR signaling promotes Treg differentiation in the absence of SCD1. **A, B** Ligand-binding luciferase reporter assays were used to assess ligation of the different PPAR isoforms ( $n = 6-12$  samples). Jurkat T cells were treated with vehicle, ATGL inhibitor (ATGLinh, atlistatin,  $20 \mu\text{M}$ ), SCD1 inhibitor (SCD1inh, CAY10566,  $10 \mu\text{M}$ ) (**A**), DHA ( $1 \mu\text{M}$ ) (**B**), and/or PPAR agonists (PPAR $\alpha^{\text{ago}}$ : WY-14643,  $10 \mu\text{M}$ ; PPAR $\beta^{\text{ago}}$ : GW501516,  $10 \mu\text{M}$ ; PPAR $\gamma^{\text{ago}}$ : rosiglitazone,  $10 \mu\text{M}$ ) for 24 h, after which PPAR ligation was assessed. **C, D** Wild-type (wt) and *Scd1*<sup>-/-</sup> naïve T cells were differentiated under Treg polarizing conditions and treated with vehicle, PPAR $\alpha$  antagonist (PPAR $\alpha^{\text{anta}}$ : GW6471,  $25 \mu\text{M}$ ;  $n = 7-13$  samples), PPAR $\beta$  antagonist (PPAR $\beta^{\text{anta}}$ : PTS58,  $25 \mu\text{M}$ ;  $n = 5-7$  samples), and PPAR $\gamma$  antagonist (PPAR $\gamma^{\text{anta}}$ : GW9662,  $25 \mu\text{M}$ ;  $n = 18-20$  samples). The frequency of CD4<sup>+</sup>FOXP3<sup>+</sup> cells was quantified one day after Treg induction. Representative flow cytometric plots (**C**) and flow cytometric analysis (**D**) are shown. **E** Human naïve T cells were differentiated under Treg polarizing conditions and treated with vehicle ( $n = 5$  healthy controls), PPAR $\alpha$  antagonist (PPAR $\alpha^{\text{anta}}$ : GW6471,  $25 \mu\text{M}$ ;  $n = 3$  healthy controls), PPAR $\beta$  antagonist (PPAR $\beta^{\text{anta}}$ : PTS58,  $25 \mu\text{M}$ ;  $n = 3$  healthy controls) or PPAR $\gamma$  antagonist (PPAR $\gamma^{\text{anta}}$ :  $25 \mu\text{M}$ ;  $n = 4$  healthy controls). The frequency of CD25<sup>+</sup>FOXP3<sup>+</sup> cells among total CD4<sup>+</sup> cells was quantified four days after Treg induction by flow cytometry. **F, G** Wt and *Scd1*<sup>-/-</sup> mice with EAE were treated daily with vehicle or a PPAR $\gamma$  antagonist (GW9662,  $2 \text{ mg/kg}$ ,  $n = 5/\text{group}$ ). Lymph nodes were collected 28 days postimmunization. EAE disease score (**F**) and flow cytometric analysis of the frequency of CD4<sup>+</sup>FOXP3<sup>+</sup> cells in the lymph nodes (**G**). Data are represented as the mean  $\pm$  SEM.  $^{**}P < 0.01$ , calculated with Tukey's post hoc analysis

In summary, our findings highlight the importance of fatty acid desaturation by SCD1 in controlling Treg differentiation and protective autoimmunity in the EAE model.

Our findings demonstrate that a lack of SCD1 increases ATGL-dependent hydrolysis of TGs and PC, resulting in elevated

intracellular levels of nonesterified DHA, activation of PPAR $\gamma$ , enhanced differentiation of Tregs, and reduced EAE disease severity. Accordingly, ATGL is reported to favor the hydrolysis of TGs and phospholipids rich in PUFAs such as DHA, and DHA is a potent endogenous ligand for PPAR $\gamma$  [38, 51]. Furthermore,



previous studies have shown that DHA and synthetic PPAR $\gamma$  agonists promote the differentiation and maintenance of Tregs and reduce neuroinflammation in experimental animal models [41, 52–57]. Surprisingly, we found that PPAR $\gamma$  antagonism reduced EAE disease severity compared to that in the control mice. The latter finding contradicts the beneficial impact of PPAR $\gamma$  agonists in the EAE model but is consistent with GW9662 displaying anti-inflammatory properties in vitro and in vivo [48]. Overall, our findings identify the SCD1-ATGL-PPAR axis as a key signaling pathway in driving Treg differentiation and highlight the complexity of PPAR signaling in (auto)immune disorders.

The molecular mechanisms that underlie the increased ATGL-dependent release of DHA in *Scd1*<sup>-/-</sup> T cells remain to be clarified. In the absence of SCD1, T cells may increase ATGL-dependent intracellular release of free DHA to protect themselves against endoplasmic reticulum stress induced by elevated levels of SFAs, potentially through activation of PPAR $\gamma$  [58, 59]. In support of this notion, pathway analysis showed that differentially expressed genes in *Scd1*<sup>-/-</sup> T cells were enriched in the canonical pathway ‘unfolded protein response’, a cellular response associated with ER stress [60]. Alternatively, or in parallel, changes in the activity or abundance of signal transducer and activator of transcription 5 (STAT5), SP1, insulin, and TNF $\alpha$  may increase ATGL expression and activity in the absence of SCD1 [61–64]. On a related note, while SFAs are generally believed to promote inflammation, our findings indicate the opposite. Lack of SCD1 enhanced Treg differentiation and suppressed neuroinflammation, despite decreasing the intracellular desaturation index. Given that PUFAs are more potent PPAR $\gamma$  agonists than MUFAs [51], elevated DHA levels may outweigh and nullify the inflammatory impact of SFAs in our study. Alternatively, while the majority of studies determined the effects of exogenous SFAs on T cell physiology, the mode of action and cellular outcome of exogenously and endogenously altered SFA levels might differ [65]. Collectively, our findings indicate that the ATGL-DHA-PPAR $\gamma$  signaling axis is essential in driving enhanced Treg differentiation in *Scd1*-deficient T cells. However, more research is warranted to define the molecular mechanisms that control the activity of the ATGL-DHA-PPAR $\gamma$  axis.

LC-ESI-MS/MS analysis demonstrated that a lack of SCD1 decreases the bulk of major fatty acid-containing lipid species in T cells without affecting cell size and granularity. Given that differentially expressed genes in *Scd1*<sup>-/-</sup> naïve T cells were enriched in pathways related to lipid efflux, these findings may reflect an increased capacity of *Scd1*<sup>-/-</sup> T cells to dispose intracellular cholesterol and phospholipids. A complementary reduction in lipogenesis and activation in lipolysis may contribute to the observed decreased lipid load in *Scd1*<sup>-/-</sup> T cells [66]. Alongside elevated intracellular levels of nonesterified DHA, LC-MS/MS analysis revealed an increased abundance of the  $\omega$ 6 PUFA AA (C20:4) and its derivatives 11-HETE and 15-HETE in *Scd1*<sup>-/-</sup> naïve T cells. Given that ATGL preferentially hydrolyses lipid species rich in PUFAs such as DHA and AA, these findings are consistent with increased ATGL activity in *Scd1*<sup>-/-</sup> naïve T cells. Of interest, previous studies demonstrated that AA and its derivatives are endogenous PPAR $\gamma$  agonists and closely associated with Treg differentiation [51, 67, 68]. To what extent AA, 11-HETE, and 15-HETE contribute to enhanced Treg differentiation in *Scd1*<sup>-/-</sup> T cells remains to be determined.

A growing body of epidemiological, preclinical, and observational studies suggests that obesity and Western diets rich in saturated fats, cholesterol, and carbohydrates are associated with Treg dysfunction, neuroinflammation, and autoimmunity [5, 6, 69–71]. Of interest, obesity and consumption of a Western diet result in markedly elevated expression and activity of hepatic SCD1 [72–74], and *Scd1*-deficient mice are protected from diet-induced obesity [75, 76]. Hence, our findings argue that SCD1 is an enzymatic driver underlying the impact of obesity and Western-type diets on immune cell imbalances and disease progression in autoimmune disorders such as MS. Vice versa, given that DHA inhibits *Scd1* expression [77], the beneficial impact of DHA supplementation on

Treg differentiation, EAE severity, and disease pathology of autoimmune disorders such as MS, systemic lupus erythematosus, and rheumatoid arthritis might depend on changes in SCD1 activity [54, 78]. Future dietary studies are warranted to unravel the causal role of SCD1 in driving the beneficial and detrimental impact of DHA and a Western diet, respectively, on the immunopathology of MS and other autoimmune disorders.

In summary, we report that SCD1 plays a crucial role in autoimmunity by suppressing Treg differentiation. Conclusions from this study extend our previous findings that SCD1 impairs the reparative properties of macrophages and microglia in the CNS [26]. Together, our findings argue that pharmacological inhibitors of SCD1 are a promising therapeutic strategy to simultaneously suppress autoimmunity, reduce neuroinflammation, and promote CNS repair. Our findings further provide a potential molecular rationale for the beneficial and detrimental impact of dietary factors on autoimmunity and validate other recent studies that identified changes in fatty acid metabolism as a crucial determinant of the pathological outcome of these factors. Finally, this study endorses the essential role of PPAR $\gamma$  in driving autoimmunity and disease progression in MS [79–83]. Altogether, our findings place SCD1 at the crossroads of autoimmunity and lipid metabolism.

## REFERENCES

- Dominguez-Villar M, Hafler DA. Regulatory T cells in autoimmune disease. *Nat Immunol.* 2018;19:665–73.
- Alissafi T, Kalafati L, Lazari M, Filia A, Kloukina I, Manifava M, et al. Mitochondrial oxidative damage underlies regulatory T cell defects in autoimmunity. *Cell Metab.* 2020;32:591–604 e597.
- Kleinenwiefeld M, Hafler DA. Regulatory T cells in autoimmune neuroinflammation. *Immunol Rev.* 2014;259:231–44.
- Bogie JFJ, Haidar M, Kooij G, Hendriks JJA. Fatty acid metabolism in the progression and resolution of CNS disorders. *Adv Drug Deliv Rev.* 2020;159:198–213.
- Swank RL, Lerstad O, Strom A, Backer J. Multiple sclerosis in rural Norway its geographic and occupational incidence in relation to nutrition. *New Engl J Med.* 1952;246:722–8.
- Alter M, Yamoore M, Harshe M. Multiple sclerosis and nutrition. *Arch Neurol.* 1974;31:267–72.
- Duscha A, Gisevius B, Hirschberg S, Yissachar N, Stangl GI, Eilers E, et al. Propionic acid shapes the multiple sclerosis disease course by an immunomodulatory mechanism. *Cell.* 2020;180:1067–1080 e1016.
- Haghikia A, Jörg S, Duscha A, Berg J, Manzel A, Waschbisch A, et al. Dietary fatty acids directly impact central nervous system autoimmunity via the small intestine. *Immunity.* 2016;44:951–3.
- Pompura SL, Wagner A, Kitz A, LaPerche J, Yosef N, Dominguez-Villar M, et al. Oleic acid restores suppressive defects in tissue-resident FOXP3 regulatory T cells from patients with multiple sclerosis. *J Clin Invest.* 2021;131:1–2.
- Kong W, Yen JH, Ganea D. Docosahexaenoic acid prevents dendritic cell maturation, inhibits antigen-specific Th1/Th17 differentiation and suppresses experimental autoimmune encephalomyelitis. *Brain, Behav, immunity.* 2011;25:872–82.
- Chiurchiù V, Leuti A, Dalli J, Jacobsson A, Battistini L, Maccarrone M, et al. Proresolving lipid mediators resolvin D1, resolvin D2, and maresin 1 are critical in modulating T cell responses. *Science translational medicine.* 2016;8:353ra111.
- Poisson LM, Suhail H, Singh J, Datta I, Denic A, Labuzek K, et al. Untargeted Plasma Metabolomics Identifies Endogenous Metabolite with Drug-like Properties in Chronic Animal Model of Multiple Sclerosis. *The Journal of biological chemistry.* 2015;290:30697–712.
- Berod L, Friedrich C, Nandan A, Freitag J, Hagemann S, Harmrolfs K, et al. De novo fatty acid synthesis controls the fate between regulatory T and T helper 17 cells. *Nature medicine.* 2014;20:1327–33.
- Young KE, Flaherty S, Woodman KM, Sharma-Walia N, Reynolds JM. Fatty acid synthase regulates the pathogenicity of Th17 cells. *Journal of leukocyte biology.* 2017;102:1229–35.
- Mørkholt AS, Oklinski MK, Larsen A, Bockermann R, Issazadeh-Navikas S, Nieland J, et al. Pharmacological inhibition of carnitine palmitoyl transferase 1 inhibits and reverses experimental autoimmune encephalitis in rodents. *PLoS One.* 2020;15:e0234493.
- Haxhinasto S, Mathis D, Benoist C. The AKT-mTOR axis regulates de novo differentiation of CD4+Foxp3+ cells. *J Exp Med.* 2008;205:565–74.
- Michalek RD, Gerriets VA, Jacobs SR, Macintyre AN, MacIver NJ, Mason EF, et al. Cutting edge: distinct glycolytic and lipid oxidative metabolic programs are

- essential for effector and regulatory CD4<sup>+</sup> T cell subsets. *J Immunol.* 2011; 186:3299–303.
18. Endo Y, Asou HK, Matsugae N, Hirahara K, Shinoda K, Tumes DJ, et al. Obesity Drives Th17 Cell Differentiation by Inducing the Lipid Metabolic Kinase, ACC1. *Cell reports.* 2015;12:1042–55.
  19. Ntambi JM. The regulation of stearoyl-CoA desaturase (SCD). *Prog Lipid Res.* 1995;34:139–50.
  20. Miyazaki M, Man WC, Ntambi JM. Targeted disruption of stearoyl-CoA desaturase1 gene in mice causes atrophy of sebaceous and meibomian glands and depletion of wax esters in the eyelid. *J Nutr.* 2001;131:2260–8.
  21. Miyazaki M, Flowers MT, Sampath H, Chu K, Oztzelberger C, Liu X, et al. Hepatic stearoyl-CoA desaturase-1 deficiency protects mice from carbohydrate-induced adiposity and hepatic steatosis. *Cell Metab.* 2007;6:484–96.
  22. Vereecke L, Vieira-Silva S, Billiet T, van Es JH, Mc Guire C, Slowicka K, et al. A20 controls intestinal homeostasis through cell-specific activities. *Nat Commun.* 2014;5:5103.
  23. Mayer N, Schweiger M, Romauch M, Grabner GF, Eichmann TO, Fuchs E, et al. Development of small-molecule inhibitors targeting adipose triglyceride lipase. *Nat Chem Biol.* 2013;9:785–7.
  24. Kleinewietfeld M, Puentes F, Borsellino G, Battistini L, Röttschke O, Falk K. CCR6 expression defines regulatory effector/memory-like cells within the CD25(+) CD4<sup>+</sup> T-cell subset. *Blood.* 2005;105:2877–86.
  25. Hernandez AL, Kitz A, Wu C, Lowther DE, Rodriguez DM, Vudattu N, et al. Sodium chloride inhibits the suppressive function of FOXP3<sup>+</sup> regulatory T cells. *J Clin Invest.* 2015;125:4212–22.
  26. Bogie JFJ, Grajchen E, Wouters E, Corrales AG, Dierckx T, Vanherle S, et al. Stearoyl-CoA desaturase-1 impairs the reparative properties of macrophages and microglia in the brain. *J Exp Med.* 2020;4:217.
  27. Nelissen K, Smeets K, Mulder M, Hendriks JJ, Ameloot M. Selection of reference genes for gene expression studies in rat oligodendrocytes using quantitative real time PCR. *J Neurosci Methods.* 2010;187:78–83.
  28. Bogie JF, Mailleux J, Wouters E, Jorissen W, Grajchen E, Vanmol J, et al. Scavenger receptor collectin placenta 1 is a novel receptor involved in the uptake of myelin by phagocytes. *Scientific Rep.* 2017;7:44794.
  29. Dobin A, Davis CA, Schlesinger F, Drenkow J, Zaleski C, Jha S, et al. STAR: ultrafast universal RNA-seq aligner. *Bioinformatics.* 2013;29:15–21.
  30. Jónasdóttir HS, Brouwers H, Kwekkeboom JC, van der Linden H, Huizinga T, Kloppenburg M, et al. Targeted lipidomics reveals activation of resolution pathways in knee osteoarthritis in humans. *Osteoarthritis Cartilage.* 2017;25:1150–60.
  31. Raspé E, Madsen L, Lefebvre AM, Leitersdorf I, Gelman L, Peinado-Onsurbe J, et al. Modulation of rat liver apolipoprotein gene expression and serum lipid levels by tetradecylthioacetic acid (TTA) via PPARalpha activation. *J Lipid Res.* 1999;40:2099–110.
  32. Carmona MC, Louche K, Lefebvre B, Pilon A, Hennuyer N, Audinot-Bouchez V, et al. S 26948: A new specific peroxisome proliferator activated receptor gamma modulator with potent antidiabetes and antiatherogenic effects. *Diabetes.* 2007;56:2797–808.
  33. Tracz-Gaszewska Z, Dobrzyn P. Stearoyl-CoA Desaturase 1 as a therapeutic target for the treatment of cancer. *Cancers (Basel).* 2019;11.
  34. Ouyang W, Beckett O, Ma Q, Paik JH, DePinho RA, Li MO. Foxo proteins cooperatively control the differentiation of Foxp3<sup>+</sup> regulatory T cells. *Nat Immunol.* 2010;11:618–27.
  35. Fontenot JD, Gavin MA, Rudensky AY. Foxp3 programs the development and function of CD4<sup>+</sup>CD25<sup>+</sup> regulatory T cells. *Nat Immunol.* 2003;4:330–6.
  36. Yao Z, Kanno Y, Kerenyi M, Stephens G, Durant L, Watford WT, et al. Nonredundant roles for Stat5a/b in directly regulating Foxp3. *Blood.* 2007;109:4368–75.
  37. Rudra D, Egawa T, Chong MM, Treuting P, Littman DR, Rudensky AY. Runx-CBFbeta complexes control expression of the transcription factor Foxp3 in regulatory T cells. *Nat Immunol.* 2009;10:1170–7.
  38. Schreiber R, Xie H, Schweiger M. Of mice and men: The physiological role of adipose triglyceride lipase (ATGL). *Biochim Biophys Acta Mol Cell Biol Lipids.* 2019;1864:880–99.
  39. German OL, Monaco S, Agnolazza DL, Rotstein NP, Politi LE. Retinoid X receptor activation is essential for docosahexaenoic acid protection of retina photoreceptors. *J Lipid Res.* 2013;54:2236–46.
  40. Grygiel-Gorniak B. Peroxisome proliferator-activated receptors and their ligands: Nutritional and clinical implications—a review. *Nutr J.* 2014;13:17.
  41. Cipolletta D, Feuerer M, Li A, Kamei N, Lee J, Shoelson SE, et al. PPAR-gamma is a major driver of the accumulation and phenotype of adipose tissue Treg cells. *Nature.* 2012;486:549–53.
  42. Brocker CN, Kim D, Melia T, Karri K, Velenosi TJ, Takahashi S, et al. Long non-coding RNA Gm15441 attenuates hepatic inflammasome activation in response to PPARA agonism and fasting. *Nat Commun.* 2020;11:5847.
  43. Xu J, Chavis JA, Racke MK, Drew PD. Peroxisome proliferator-activated receptor-alpha and retinoid X receptor agonists inhibit inflammatory responses of astrocytes. *J Neuroimmunol.* 2006;176:95–105.
  44. Lohakare J, Osorio JS, Bionaz M. Peroxisome proliferator-activated receptor  $\beta/\delta$  does not regulate glucose uptake and lactose synthesis in bovine mammary epithelial cells cultivated in vitro. *J Dairy Res.* 2018;85:295–302.
  45. Naruhn S, Toth PM, Adhikary T, Kaddatz K, Pape V, Dörr S, et al. High-affinity peroxisome proliferator-activated receptor  $\beta/\delta$ -specific ligands with pure antagonistic or inverse agonistic properties. *Mol Pharmacol.* 2011;80:828–38.
  46. Baumann A, Burger K, Brandt A, Staltner R, Jung F, Rajcic D, et al. GW9662, a peroxisome proliferator-activated receptor gamma antagonist, attenuates the development of non-alcoholic fatty liver disease. *Metabolism.* 2022; 133:155233.
  47. Natarajan C, Bright JJ. Peroxisome proliferator-activated receptor-gamma agonists inhibit experimental allergic encephalomyelitis by blocking IL-12 production, IL-12 signaling and Th1 differentiation. *Genes Immun.* 2002;3:59–70.
  48. Bei Y, Chen J, Zhou F, Huang Y, Jiang N, Tan R, et al. BZ-26, a novel GW9662 derivative, attenuated inflammation by inhibiting the differentiation and activation of inflammatory macrophages. *Biomed Pharmacother.* 2016;84:730–9.
  49. Son YM, Cheon IS, Goplen NP, Dent AL, Sun J. Inhibition of stearoyl-CoA desaturases suppresses follicular help T- and germinal center B- cell responses. *Eur J Immunol.* 2020;50:1067–77.
  50. Yeoh BS, Saha P, Singh V, Xiao X, Ying Y, Vanamala JK, et al. Deficiency of stearoyl-CoA desaturase-1 aggravates colitogenic potential of adoptively transferred effector T cells. *Am J Physiol Gastrointest Liver Physiol.* 2016;311:G713–G723.
  51. Echeverria F, Ortiz M, Valenzuela R, Videla LA. Long-chain polyunsaturated fatty acids regulation of PPARs, signaling: Relationship to tissue development and aging. *Prostaglandins Leukot Essent Fatty Acids.* 2016;114:28–34.
  52. Kim JY, Lim K, Kim KH, Kim JH, Choi JS, Shim SC. N-3 polyunsaturated fatty acids restore Th17 and Treg balance in collagen antibody-induced arthritis. *PLoS One.* 2018;13:e0194331.
  53. Bi X, Li F, Liu S, Jin Y, Zhang X, Yang T, et al. omega-3 polyunsaturated fatty acids ameliorate type 1 diabetes and autoimmunity. *J Clin Invest.* 2017;127:1757–71.
  54. Adkins Y, Soulika AM, Mackey B, Kelley DS. Docosahexaenoic acid (22:6n-3) Ameliorated the onset and severity of experimental Autoimmune Encephalomyelitis in Mice. *Lipids.* 2019;54:13–23.
  55. Wohlfert EA, Nichols N, Nevius E, Clark RB. Peroxisome proliferator-activated receptor gamma (PPARgamma) and immunoregulation: enhancement of regulatory T cells through PPARgamma-dependent and -independent mechanisms. *J Immunol.* 2007;178:4129–35.
  56. Guri AJ, Mohapatra SK, Horne WT 2nd, Hontecillas R, Bassaganya-Riera J. The role of T cell PPAR gamma in mice with experimental inflammatory bowel disease. *BMC Gastroenterol.* 2010;10:60.
  57. Park HJ, Kim DH, Choi JY, Kim WJ, Kim JY, Senejani AG, et al. PPARgamma negatively regulates T cell activation to prevent follicular helper T cells and germinal center formation. *PLoS One.* 2014;9:e99127.
  58. Begum G, Harvey L, Dixon CE, Sun D. ER stress and effects of DHA as an ER stress inhibitor. *Transl Stroke Res.* 2013;4:635–42.
  59. Shen X, Yang L, Yan S, Zheng H, Liang L, Cai X, et al. Fetuin A promotes lipotoxicity in beta cells through the TLR4 signaling pathway and the role of pioglitazone in anti-lipotoxicity. *Mol Cell Endocrinol.* 2015;412:1–11.
  60. Grootjans J, Kaser A, Kaufman RJ, Blumberg RS. The unfolded protein response in immunity and inflammation. *Nat Rev Immunol.* 2016;16:469–84.
  61. Kaltenecker D, Mueller KM, Benedikt P, Feiler U, Themanns M, Schleder M, et al. Adipocyte STAT5 deficiency promotes adiposity and impairs lipid mobilisation in mice. *Diabetologia.* 2017;60:296–305.
  62. Roy D, Farabaugh KT, Wu J, Charrier A, Smas C, Hatzoglou M, et al. Coordinated transcriptional control of adipocyte triglyceride lipase (Atgl) by transcription factors Sp1 and peroxisome proliferator-activated receptor gamma (PPARgamma) during adipocyte differentiation. *J Biol Chem.* 2017; 292:14827–35.
  63. Chakrabarti P, Kim JY, Singh M, Shin YK, Kim J, Kumbrink J, et al. Insulin inhibits lipolysis in adipocytes via the evolutionarily conserved mTORC1-Egr1-ATGL-mediated pathway. *Mol Cell Biol.* 2013;33:3659–66.
  64. Kim JY, Tillison K, Lee JH, Rearick DA, Smas CM. The adipose tissue triglyceride lipase ATGL/PNPLA2 is downregulated by insulin and TNF-alpha in 3T3-L1 adipocytes and is a target for transactivation by PPARgamma. *Am J Physiol Endocrinol Metab.* 2006;291:E115–127.
  65. Schweitzer SC, Reding AM, Patton HM, Sullivan TP, Stubbs CE, Villalobos-Menuet E, et al. Endogenous versus exogenous fatty acid availability affects lysosomal acidity and MHC class II expression. *J Lipid Res.* 2006;47:2525–37.
  66. Bednarski T, Olichwier A, Opasinska A, Pyrkowska A, Gan AM, Ntambi JM, et al. Stearoyl-CoA desaturase 1 deficiency reduces lipid accumulation in the heart by activating lipolysis independently of peroxisome proliferator-activated receptor alpha. *Biochimica et Biophysica Acta.* 2016;1861:2029–37.
  67. Baratelli F, Lin Y, Zhu L, Yang SC, Heuzé-Vourc'h N, Zeng G, et al. Prostaglandin E2 induces FOXP3 gene expression and T regulatory cell function in human CD4<sup>+</sup> T cells. *J Immunol.* 2005;175:1483–90.

68. Powell WS, Rokach J. Biosynthesis, biological effects, and receptors of hydroxyicosatetraenoic acids (HETEs) and oxoicosatetraenoic acids (oxo-ETEs) derived from arachidonic acid. *Biochimica et Biophysica Acta*. 2015;1851:340–55.
69. Matveeva O, Bogie J, Hendriks J, Linker RA, Haghikia A, Kleinewietfeld M. Western lifestyle and immunopathology of multiple sclerosis. *Ann NY Acad Sci*. 2018;1417(Apr):71–86.
70. Timmermans S, Bogie JF, Vanmierlo T, Lütjohann D, Stinissen P, Hellings N, et al. High fat diet exacerbates neuroinflammation in an animal model of multiple sclerosis by activation of the Renin Angiotensin system. *J Neuroimmune Pharmacol*. 2014;9:209–17.
71. Wagner NM, Brandhorst G, Czepluch F, Lankeit M, Eberle C, Herzberg S, et al. Circulating regulatory T cells are reduced in obesity and may identify subjects at increased metabolic and cardiovascular risk. *Obesity (Silver Spring)*. 2013;21:461–8.
72. Biddinger SB, Almind K, Miyazaki M, Kokkotou E, Ntambi JM, Kahn CR. Effects of diet and genetic background on sterol regulatory element-binding protein-1c, stearoyl-CoA desaturase 1, and the development of the metabolic syndrome. *Diabetes*. 2005;54:1314–23.
73. Flowers MT, Ntambi JM. Stearoyl-CoA desaturase and its relation to high-carbohydrate diets and obesity. *Biochimica et Biophysica Acta*. 2009;1791:85–91.
74. Hu CC, Qing K, Chen Y. Diet-induced changes in stearoyl-CoA desaturase 1 expression in obesity-prone and -resistant mice. *Obes Res*. 2004;12:1264–70.
75. O'Neill LM, Phang YX, Matango M, Shamsuzzaman S, Guo CA, Nelson DW, et al. Global deficiency of stearoyl-CoA desaturase-2 protects against diet-induced adiposity. *Biochem Biophys Res Commun*. 2020;527:589–95.
76. Miyazaki M, Sampath H, Liu X, Flowers MT, Chu K, Dobrzyn A, et al. Stearoyl-CoA desaturase-1 deficiency attenuates obesity and insulin resistance in leptin-resistant obese mice. *Biochem Biophys Res Commun*. 2009;380:818–22.
77. Bellenger J, Bellenger S, Clément L, Mandard S, Diot C, Poisson JP, et al. A new hypotensive polyunsaturated fatty acid dietary combination regulates oleic acid accumulation by suppression of stearoyl CoA desaturase 1 gene expression in the SHR model of genetic hypertension. *FASEB J*: Official publication of the Federation of American Societies for Experimental Biology. 2004;18:773–5.
78. Li X, Bi X, Wang S, Zhang Z, Li F, Zhao AZ. Therapeutic Potential of omega-3 Polyunsaturated Fatty Acids in Human Autoimmune Diseases. *Front Immunol*. 2019;10:2241.
79. Shukla DK, Kaiser CC, Stebbins GT, Feinstein DL. Effects of pioglitazone on diffusion tensor imaging indices in multiple sclerosis patients. *Neurosci Lett*. 2010;472:153–6.
80. Kaiser CC, Shukla DK, Stebbins GT, Skias DD, Jeffery DR, Stefoski D, et al. A pilot test of pioglitazone as an add-on in patients with relapsing remitting multiple sclerosis. *J Neuroimmunol*. 2009;211:124–30.
81. Pershadsingh HA, Heneka MT, Saini R, Amin NM, Broeske DJ, Feinstein DL. Effect of pioglitazone treatment in a patient with secondary multiple sclerosis. *J Neuroinflammation*. 2004;1:3.
82. Drew PD, Xu J, Racke MK. PPAR-gamma: Therapeutic potential for multiple sclerosis. *PPAR Res*. 2008;2008:627463.
83. International Multiple Sclerosis Genetics Consortium. Multiple sclerosis genomic map implicates peripheral immune cells and microglia in susceptibility. *Science*. 2019;365:eav7188.

## ACKNOWLEDGEMENTS

We thank MP Tulleners for excellent technical assistance. We would also like to thank other members of the Biomedical Research Institute (Hasselt University) for providing feedback and suggestions during the preparation of the manuscript.

## AUTHOR CONTRIBUTIONS

EG, ML, MH, MK, JJA, and JFB conceived the experiments. EG, PB, BFC-R, ML, SV, JD, JYB, LVZ, and JFB performed the experiments. EG, PB, ML, IH, MH, SGSV, JD, JYB, and JFB analyzed the data. EG, PB, BFC-R, ML, IH, MH, JD, JYB, MG, LVZ, JMN, NH, GK, RZ, RB, JVS, BB, MK, JJA, and JFB discussed the results. JMN, PS, NH, MG, RZ, RB, GK, and MK contributed reagents, materials, and analysis tools. EG, MH, JJA, and JFB wrote the manuscript. EG, PB, BFC-R, ML, IH, SV, MH, SGSV, JD, JYB, LVZ, JMN, PS, NH, MG, RZ, RB, GK, JVS, BB, MK, JJA, and JFB revised the manuscript.

## FUNDING

The work has been supported by the Flemish Fund for Scientific Research (FWO Vlaanderen; 12J9116N, 12JG119N, 12U7718N, 1S15519N, and G099618N), the Belgian Charcot Foundation (FCS-2016-EG7, R-8676, and R-6832), the Interreg V-A EMR program (EURLIPIDS, EMR23), and the special research fund UHasselt (BOF). JMN is supported by a National Institutes of Health Grant (R01 DK062388). MK was supported by the European Research Council (ERC) under the European Union's Horizon 2020 research and innovation program (640116) and by a SALK grant from the government of Flanders and by an Odysseus grant of the Research Foundation Flanders, Belgium (FWO).

## COMPETING INTERESTS

The authors declare no competing interests.

## ADDITIONAL INFORMATION

**Supplementary information** The online version contains supplementary material available at <https://doi.org/10.1038/s41423-023-01011-2>.

**Correspondence** and requests for materials should be addressed to Jeroen F. J. Bogie.

**Reprints and permission information** is available at <http://www.nature.com/reprints>



**Open Access** This article is licensed under a Creative Commons Attribution 4.0 International License, which permits use, sharing, adaptation, distribution and reproduction in any medium or format, as long as you give appropriate credit to the original author(s) and the source, provide a link to the Creative Commons license, and indicate if changes were made. The images or other third party material in this article are included in the article's Creative Commons license, unless indicated otherwise in a credit line to the material. If material is not included in the article's Creative Commons license and your intended use is not permitted by statutory regulation or exceeds the permitted use, you will need to obtain permission directly from the copyright holder. To view a copy of this license, visit <http://creativecommons.org/licenses/by/4.0/>.

© The Author(s) 2023